Single-cell analysis characterizes PLK1 as a promoter of immunosuppressive tumor microenvironment in LUAD

Yifan Kong[1, 5], Chaohao Li[1, 5], Jinpeng Liu[3], Min Zhang[1], Derek B. Allison[4], Faisal Hassan[4], Daheng He[3], Xinyi Wang[1], Fengyi Mao[1], Qiongsi Zhang[1], Yanquan Zhang[1], Zhiguo Li[1], Sai Wu[1], Chi Wang[2, 3] and Xiaoqi Liu[1, 3*]

[1]Department of Toxicology and Cancer Biology, University of Kentucky, Lexington, KY, 40536

[2]Department of Biostatistics, University of Kentucky, Lexington, KY, 40536

[3]Markey Cancer Center, University of Kentucky, Lexington, KY, 40536

[4]Department of Pathology and Laboratory Medicine, University of Kentucky, Lexington, KY, 40536

[5]These authors contribute equally.

Running title: PLK1 promotes immunosuppressive TME.

Keywords: PLK1, LUAD, TME, single-cell RNA-seq, MHC-II.

Conflict of Interest: The authors declare no conflict of interest.

*** To whom correspondence should be addressed:**

Dr. Xiaoqi Liu: Department of Toxicology and Cancer Biology, University of Kentucky, Lexington, KY, 40536. Phone: 859-562-2006; Fax: 859-323-1059; Email: xiaoqi.liu@uky.edu

Abstract

PLK1 (Polo-like kinase 1) plays a critical role in cancer progression of lung adenocarcinoma (LUAD). Recent studies have demonstrated that targeting PLK1 improves the efficacy of immunotherapy, indicating its important role in the regulation of tumor immunity. However, the correlation between PLK1 and tumor microenvironment (TME) is poorly understood. Here, using genetically engineered mouse model and single-cell RNA-seq analysis, we report that PLK1 promotes a general immunosuppressive TME in LUAD characterized with impaired tumor-infiltrating lymphocytes, enhanced M2 polarization and suppression of antigen presentation process. Mechanistically, elevated PLK1 coincides with increased secretion of CXCL2 cytokine, which promotes M2 polarization of macrophages and decreases expression of class II major histocompatibility complex (MHC-II) in professional antigen-presenting cells. Furthermore, PLK1 negatively regulates MHC-II expression in cancer cells, which has been shown to be associated with poor tumor immunity and patients' outcomes. Taken together, our results reveal PLK1 as a novel modulator of TME in LUAD and provide possible therapeutic interventions.

Significance

The characterization of PLK1 as a promoter of immunosuppressive tumor microenvironment enhances our understanding of PLK1's role in anti-tumor immunity and supports the idea of targeting PLK1 in cancer treatment.

Introduction

Lung cancer accounts for one-fifth of all cancer mortalities in the US, making it the leading cause of cancer-related deaths [1]. Lung adenocarcinoma (LUAD) is the major type of this disease, comprising almost half of all cases [2]. LUAD is characterized by genetic alternations that drive tumor heterogeneity and the most common forms are mutations involved in receptor tyrosine kinase pathways, including EGFR, KRAS, ALK, and ROS1 genes [3]. These mutations have been demonstrated to have significant impact on disease progression and patients' response to treatment. Hence, targeted therapies have been developed for individualized treatment. Despite the advances in treatment options, the prognosis for LUAD remains poor, with the 5-year survival rate for metastatic disease is less than 5%. Therefore, precise early screening and the development of more effective treatment options are essential to improve patients' outcomes.

Recently, immunotherapies have emerged as a novel treatment option for LUAD [4]. Drugs that target the immune checkpoint have shown significant benefit to manage disease by reinvigorating the tumor immunity and allowing immune system to attack cancer cells. While immunotherapies marks the new era of cancer treatment, the success of immunotherapies depends on several factors, including the patient's immune status, and most importantly, the characteristics of the tumor microenvironment (TME), which has emerged as a pivotal area of cancer research [5]. The TME is composed of various types of tumor-infiltrating myeloid cells and lymphocytes. The interactions between cancer cells and immune cells shape the properties of tumor growth, invasion, and metastasis. More closely, immunosuppressive TME can render immunotherapies ineffective. Unfortunately, most patients don't respond to immunotherapy [6, 7]. Specifically for lung cancer, only 20% of patients respond to monotherapy with checkpoint blockade, and this number increases to 40% when combined with standard chemotherapy [8, 9], suggesting a more complex yet

underexplored features of TME in LUAD. Therefore, a better understanding of the TME is critical for developing effective immunotherapies.

Polo-like kinase 1 (PLK1) is a serine/threonine kinase that plays a critical role in various cellular processes. The canonical function of PLK1 largely focuses on the regulation of cell division at multiple phases [10-15]. Beyond its canonical role, studies have identified several non-mitotic functions of PLK1, including the regulation of DNA damage repair, metabolism, and immune response [16]. Due to the wide involvement of PLK1 in many critical biological events, Dysregulation of PLK1 has been implicated in tumorigenesis, with elevated expression observed in various types of cancers [17]. Considering its importance in tumorigenesis, novel therapies targeting PLK1 have been developed with observable efficacy in cell and animal models [18]. Both our lab and others have proven that PLK1 overexpression in LUAD leads to cancer progression and associates with poor overall survival [19, 20]. Interestingly, recent studies have validated PLK1 as a potential target to improve the efficacy of immunotherapies in lung cancer [21], consistent with our finding in pancreatic cancer that targeting PLK1 in pancreatic cancer enhances the effectiveness of immune checkpoint blockade [22]. While these results indicate that PLK1 may be an important modulator of tumor immunity, whether and how PLK1 functions in the TME of LUAD is largely unknown. Here, using single-cell sequencing, we show that elevation of PLK1 incurs a suppressive TME in LUAD, marked by decreased infiltration of immune cells, M2 polarization and suppression of antigen presentation process. Elevation of PLK1 promotes M2 polarization and attenuates the expression of class II major histocompatibility complex (MHC-II) in professional antigen presentation cells and cancer cells, leading to impaired antigen presentation and anti-tumor immunity. Our results reveal PLK1 as a key regulator of TME and provide evidence of targeting PLK1 to improve immunotherapies in LUAD.

101 **Methods**

102 **Sample preparation for single-cell sequencing**

103 All animal experiments used in this study were approved by the University of Kentucky Division
104 of Laboratory Animal Resources. 8-week-old LSL-Kras^{G12D}/Tp53$^{f/f}$ (KP) and LSL-
105 Kras^{G12D}/Tp53$^{f/f}$/LSL-Plk1 (KPP) mice were intratracheally instilled with adenovirus-expressing
106 Cre recombinase at a viral titer of 2.5×10^7 PFU per mouse according to the protocol [23]. Tumor
107 formations were monitored every week by MRI and harvested after 12 weeks of adenovirus
108 delivery. Single cell suspensions were prepared following 10x Genomics Cell Preparation Guide.
109 Briefly, mice lung tissues were harvested and cut into smaller pieces, then used pipette to
110 extensively pipette up and down to get tissue mixture in DMEM medium containing 2% FBS. This
111 mixture was filtered with a 70 μm nylon mesh strainer, centrifuged at 300g for 10 mins, then
112 resuspended in DMEM medium containing 2% FBS to get single cell suspension. The single cell
113 suspension was further sorted to enrich immune cell populations, and this suspension was used for
114 single-cell sequencing. Cell viability was at least 95% for all samples. 10000 cells were targeted
115 for sequencing and loaded onto a Chromium Controller (10x Genomics) for gel beads-in-emulsion
116 formation. Library preparation was conducted using Chromium Next GEM Single Cell 3' Gene
117 Expression Kit (v3.1, 10x Genomics) according to the manufacturer's instructions. Single indexed,
118 paired-end libraries were sequenced on an HiSeq 2500 sequencer (Illumina).

119 **Analysis of single-cell RNA-seq**

120 Single-cell RNA-seq gene expression libraries were mapped to mm10 mouse reference (10x
121 Genomics pre-built reference, mm10-2020-A) using Cell Ranger (v6.1.1, 10x Genomics). For each
122 library, Cell Ranger filtered matrix was subjected to QC filters to remove low quality cells with

123 ⩽ 500 features or percentage of mitochondrial transcripts ⩾ 15. DoubletFinder analysis was then
124 performed on each library separately to identify and filter potential doublets with default
125 parameters [24]. Additionally, cells with features > 8000 or counts > 50,000 were removed. Pass
126 QC cells from the KP and KPP groups were combined and processed using the Seurat (v3) R
127 package [25]. Count matrices were Log-normalized and scaled. The top 2,000 highly variable
128 genes (HVGs) were selected to define principal components (PCs). Batch integration was
129 performed via Harmony algorithm (v0.1.0) to the combined data for batch effect corrections with
130 default settings [26]. Neighbor analysis was performed by FindNeighbors function using the PCs
131 from the Harmony dimension. Clustering was identified with FindClusters function at resolution
132 = 0.8. UMAP was calculated based on the Harmony dimension for clusters visualization.
133 Identification of cluster markers was performed using a Wilcoxon rank-sum test by comparing
134 each cluster with the rest of the cells. For differential gene expression analysis for each cell
135 population, we used DESeq2 test in Seurat [27], to identify the up/down-regulated sets of genes
136 between treatment groups in the cell populations. Gene Set Enrichment Analysis (GSEA) was
137 performed with fgsea R package [28], using KEGG and HALLMARK datasets [29, 30]. The two-
138 sample binomial test will be used to compare the distribution of cell clusters between the two
139 groups.

140 **Analysis of public dataset and bulky RNA-seq**

141 For STRING analysis [31], genes functionally associated with CXCL2 were directly checked with
142 online STRING tool (https://string-db.org/). For gene expressions, correlation, and survival
143 analyses of TCGA-LUAD dataset, patients' demographic data with RSEM and zscore values
144 (normalized to all samples) of gene expressions were downloaded from cBioportal [32-34].
145 Analysis of bulky RNA-seq data from KP and KPP tumors was described previously [20].

146 **Cell culture**

147 KP and KPP cell lines were isolated from transgenic mice 12–14 weeks after adenovirus infection,
148 which was described before [20]. H358 cell line was purchased from ATCC (CRL-5807). All cell
149 lines were cultured in RPMI 1640 medium containing 10% FBS, 1% penicillin-streptomycin at
150 37°C incubator with 5% CO_2. For preparation of conditioned medium, KP or KPP cells were
151 cultured in 100mm dish until 70-80% confluency, them medium was refreshed with DMEM
152 containing 0.5% FBS and continued to culture for 48h. The resulting conditioned medium was
153 used for coculture experiments and mouse cytokines array. For transfection of siRNA, predesigned
154 siRNA (Sigma) targeting PLK1 were transfected with jetPRIME Versatile DNA/siRNA
155 transfection reagent (Polyplus, 101000001) according to the manufacturer's instructions. 48h after
156 transfection, cells were harvested for subsequent experiments. All the cell lines were within 50
157 passages and tested negative for mycoplasma contamination.

158 **Coculture experiments**

159 Macrophages and dendritic cells were isolated from the bone marrows of B6 hosts. Briefly, bone
160 marrows were flushed out of the femur and tibia with complete DMEM medium using 25-gauge
161 needles. After centrifugation at 400g for 5 mins, bone marrows suspension was treated with 1x
162 RBC lysis buffer (Thermo, 00-4333-57) and centrifuged again. The cell pellets were then washed
163 with 1x PBS twice and resuspended in refresh complete DMEM medium. Cells were cultured at
164 37°C incubator with 5% CO_2 for a week to induce differentiation. For induction of macrophages,
165 cells were treated with 10ng/ml Csf1. For induction of dendritic cells were treated with 10ng/ml
166 Csf2 and 20ng/ml Il-4. Medium was changed every two days with refresh cytokines. For coculture
167 with cells, KP or KPP cells were directly seeded onto the same plates containing immune cells at
168 indicated ratio for 48h. Treatment with Cxcl2 or SX-682 started at 6h post coculture and continued

169 until end of the experiments. For coculture with conditioned medium, the conditioned medium
170 from KP or KPP, with mouse IgG or anti-Cxcl2 neutralization antibodies, was used to replace
171 normal culture medium in immune cells and continued to culture for 48h.

172 **Flow cytometry**

173 Cells were harvested by a cell scraper and washed once with 1x PBS, then stained on ice with
174 indicated antibodies (1:1000) in 1x PBS for 30mins. Samples containing tumor cells were fixed
175 with 70% ethanol before staining. Data were acquired on the BD Symphony A3 analyzer (BD
176 Biosciences) and analyzed using FlowJo software.

177 **Mouse cytokines array**

178 Mouse cytokines array experiment was performed using Proteome Profiler Mouse Cytokine Array
179 Kit (R&D Systems, ARY006) according to the manufacturer's instructions. Briefly, conditioned
180 medium from KP and KPP was incubated with membranes containing pre-adsorbed primary
181 antibodies targeting mouse cytokines. Following wash step, the membranes were then incubated
182 with HRP-linked secondary antibodies. After washing membranes again, membranes were probed
183 with chemiluminescent reagents to visualize cytokines. Medium containing 0.5% FBS but without
184 cancer cells was used as negative control. Images were captured with ChemiDoc Imaging System
185 (Bio-Rad).

186 **Immunohistochemistry (IHC)**

187 Formalin-Fixed Paraffin-Embedded slides prepared from KP and KPP tumors were stained with
188 MHC-II antibodies. IHC staining was performed with the VECTASTAIN Elite ABC Universal
189 PLUS Kit (Vector Laboratories, PK-8200) according to the manufacturer's instructions. Staining

190 was visualized with ImmPACT DAB Substrate Kit (Vector Laboratories, SK-4105) and
191 counterstained with Harris's hematoxylin.

192 **Statistical analysis**

193 Statistical analyses were performed with the statistical functions in GraphPad Prism 8 and R
194 programming language. Unless denoted elsewhere, an unpaired two-sided t test was used as the
195 default method for results. Normality and variance of results were checked to confirm the
196 requirements of t test. Statistical significance was set at $p < 0.05$ unless denoted otherwise. More
197 details can be found in the corresponding figure legends.

198

199 **Results**

200 **Elevation of PLK1 in LUAD is associated with general immunosuppressive TME.**

201 To investigate the impact of PLK1 on lung cancer TME, we designed a workflow (**Fig. 1A**) to
202 perform the single-cell RNA-seq using our LSL-Kras^{G12D}/Tp53$^{f/f}$ (KP) and LSL-
203 Kras^{G12D}/Tp53$^{f/f}$/LSL-Plk1 (KPP) mouse models that were previously reported [20]. Preliminary
204 examination of single-cell results indicated that over 95% of cells were immune cells,
205 demonstrating the efficacy and reliability of single-cell data. Unsupervised clustering of total cells
206 generated 27 different cell populations in samples (**Figs. S1A-S1B**) characterized by a specific
207 gene signature, indicating a significant intratumoral heterogeneity of cell populations. Of note, the
208 different proportion of cell populations suggested a distinct TME in KP and KPP (**Figs. S1C-S1D**).
209 In both groups, macrophages were the major population, suggesting the unique function of them
210 in lung cancer progression. To better visualize the differences in immune cell populations, we
211 performed a supervised clustering of major immune cell types based on their specific gene

212 signatures (**Figs. 1B, S1E**). Results showed that KPP tumors had low proportions of all cell types
213 except for macrophages compared to KP tumors (**Figs. 1C-1D**), indicating a general
214 immunosuppressive TME in KPP tumors. Since T cells are the major immune cells exerting direct
215 anti-tumor immunity, we further looked into T cell populations by clustering of total T cells in KP
216 and KPP tumors (**Figs. S2A-S2B**). Clearly, KPP tumors displayed decreased tumor infiltrating T
217 cells of all subtypes (**Figs. S2C-S2D**). The low levels of cytotoxic Cd8 T cells and NK cells in
218 KPP tumors were impactful, as they were the major immune cells responsible for eliminating
219 tumors, and KPP tumors were specifically protected from this anti-tumor immunity. Taken
220 together, these results illustrated that high PLK1 in LUAD promoted a general suppressive
221 immunophenotype.

222

223 **Tumor promoting M2 macrophages propagate in high PLK1 TME of LUAD.**

224 The higher proportion of tumor associated macrophages (TAM) in KPP tumors was intriguing
225 (**Figs. 1C-1D**), and this phenomenon enticed us to investigate the role of TAM in TME. Given that
226 the functions of TAM were dichotomous, we specially focused on the proportions of M1 and M2
227 macrophages in KP and KPP tumors, which were tumor suppressing and tumor promoting,
228 respectively. Analysis of gene expressions in TAM identified 1201 differentially expressed genes
229 between KP and KPP tumors (**Fig. 2A**). Investigation of top 10 up and down regulated genes in
230 KPP tumors revealed that macrophages in KPP tumors were enriched for previously validated
231 genes associated with M2 macrophages (e.g., Chil3, Ccn3) [35, 36], suggesting more M2
232 macrophages in KPP tumors (**Fig. 2B**). Examination of several M1 markers (Il1b, Tlr2, Cd86,
233 Cd68, Cd80, Socs3, Gch1) and M2 markers (Fn1, Pparg, Arg1, Slco2b1, Ptgs1, Pygl, Cd206)
234 further provided evidence for increased M2 macrophages in KPP tumors (**Fig. 2C**). To confirm

235 this phenotype, we performed supervised clustering of total macrophages, and the results indeed
236 showed that TME of KPP tumors consisted of more M2 macrophages compared to KP tumors
237 (**Figs. 2D-2E**), consistent with the observation of more suppressive immunophenotype in KPP
238 tumors. In sum, these results supported the notion that high PLK1 was associated with increased
239 tumor promoting M2 macrophages in LUAD.

240

241 **High PLK1 suppresses antigen presentation pathway and induces M2 polarization.**

242 Since high PLK1 was associated with increased infiltration and differentiation of M2 macrophages,
243 we sought to delineate the biological consequence of this phenotype and linked it with specific
244 immune cells functions. To achieve this aim, we performed GSEA in macrophages. The results
245 showed that multiple pathways associated with the functions of macrophages were dramatically
246 disturbed (**Figs. 3A-3B**). Several pathways related to immune response were suppressed in KPP
247 tumors, such as pathways associated with inflammation (e.g., IFN-γ response, **Fig. 3B**), pathogen
248 defense (e.g., viral myocarditis) and autoimmune diseases (e.g., systemic lupus erythematosus). In
249 addition, several pathways associated with steroid and lipid metabolism were elevated in KPP
250 tumors (e.g., steroid biosynthesis), which were previously demonstrated to promote M2
251 polarization [37]. These results suggested an impaired anti-tumor immune system and were in
252 agreement with the more immunosuppressive phenotype in KPP tumors. Of note, antigen
253 processing and presentation pathway was among the most suppressed pathway in macrophages.
254 Moreover, results of GSEA in other immune cells showed that inhibition of antigen processing
255 and presentation was a shared consequence among all major immune cell populations (**Fig. S3**).
256 Professional antigen presentation cells such as macrophages rely on class II major
257 histocompatibility complex (MHC-II) and costimulatory factors for their antigen processing and

258 presentation function [38]. Indeed, review of gene expressions and macrophages markers (**Figs.**
259 **2A-2C**) showcased that macrophages in KPP tumors expressed lower level of MHC-II genes
260 (Cd74, H2-Eb1, H2-Ab1) and several costimulatory factors (Cd86, Cd80), consistent with the
261 impaired antigen presentation function in this group. Given that this pathway was key to successful
262 anti-tumor immunity [39], the loss of antigen presentation function in immune cells of KPP tumors,
263 especially in M2 macrophages, further confirmed the immune suppression role of PLK1. Based
264 on these results, we hypothesized that PLK1 expression could inhibit antigen presentation and
265 polarize macrophages towards M2 subtype. To validate our hypothesis, we performed in vitro
266 coculture experiments using established cell lines from KP and KPP mice and used flow cytometry
267 to monitor expressions of important genes and markers in antigen presentation and macrophages
268 polarization. Short-term coculture of bone marrow derived macrophages (BMDM) with KP or
269 KPP showed that both cells elevated costimulatory factors (Cd80 and Cd86) with even stronger
270 effect from KPP group. However, only KPP cells were able to induce higher level of M2 marker
271 Cd206. Coculture with both cell lines attenuated MHC-II expression, suggesting potential immune
272 suppression mechanism of tumors. Compared to KP, the level of MHC-II was lower in KPP group
273 (**Figs. 3C-3D**). Given that MHC-II plays a pivotal role in antigen processing and presentation, the
274 lower expression of MHC-II in KPP group confirmed that antigen presentation function was
275 specifically dysregulated in high PLK1 condition. Collectively, these data demonstrated that PLK1
276 suppresses antigen presentation pathway and induces M2 polarization in LUAD.

277

278 **Immunosuppressive function of PLK1 depends on CXCL2.**

279 Paracrine signaling through the release of cytokines from cancer cells is critical for intercellular
280 communication and shaping anti-tumor immunity [40]. Inspection of pathway analyses in immune

281 cells revealed that several cytokine and chemokine pathways were altered (e.g., interferon response
282 pathway), and this led to our hypothesis that PLK1 suppressed anti-tumor immunity via regulation
283 of cytokine secretion. To test our hypothesis, we performed a cytokines array of mouse cytokines
284 released from the conditioned medium of KP and KPP cells. We found that cytokine profile was
285 indeed different between KP and KPP. Compared to KP, KPP cells secreted more Il-6, Cxcl2 and
286 Ccl3 cytokines, but less Ccl5 (**Fig. 4A**). The increased secretion of Il-6 was reasonable given its
287 established role in M2 polarization [41]. Besides, Ccl3 (macrophage inflammatory protein 1-alpha)
288 was one of the cytokines released from macrophages and Ccl5 was responsible for T cells
289 chemotaxis [42, 43], so their alternation was congruent with the higher proportion of macrophages
290 and lower infiltration of T cells in KPP tumors. We were especially interested in Cxcl2, as it was
291 the most highly secreted cytokine in the supernatant of KPP. It has been shown that secreted
292 CXCL2 in TME can recruit myeloid derived suppressor cells and M2 macrophages [44, 45]**,** and
293 this leads to suppression anti-tumor response (**Fig. 4B**). We also investigated which pathway was
294 responsible for the increased secretion of IFN-γ in KPP. A preliminary STRING analysis in human
295 and mice identified several important genes related to CXCL2 (**Figs. S4A**). Except for some
296 known interaction genes (e.g., CXCR1 and CXCR2, two receptors for CXCL2), we found that in
297 both species the genes related to JAK-STAT3 pathway (e.g., IL-6) and NFKB pathway (e.g., TNF,
298 Rela) commonly emerged. GSEA of RNA-seq data confirmed that two pathways were highly
299 active in KPP cells (**Fig. S4B**). Of note, although not very striking, Il-6 was simultaneously
300 detected with Cxcl2 in the secretion profile of KPP, which was not observed in KP control (**Fig.**
301 **4A**). These results provided evidence that IL-6/JAK/STAT3 and TNF/NFKB axis might account
302 for the increased Cxcl2 in KPP cells.

303 In mice, Cxcl2 can bind to Cxcr1 and Cxcr2, albeit with much higher affinity to Cxcr2 [46]. Given
304 that Cxcl2 was predominant in KPP secreted cytokines and its established role in recruiting M2
305 macrophages, we hypothesized that the observed immunosuppressive function of PLK1 depended
306 on CXCL2. To test this assumption, we performed coculture experiments of BMDM with
307 conditioned medium from KP or KPP, treated with recombinant mouse Cxcl2 or SX-682 (**Figs.**
308 **4C-4D**), a previously reported dual CXCR1/CXCR2 inhibitor in clinical trial [47]. Coculture of
309 BMDM with conditioned medium recapitulated most of the results from coculturing with cells,
310 but MHC-II was not decreased. Instead, MHC-II elevated under this condition, indicating that the
311 decrease of MHC-II in coculture with cells directly came from interaction between cancer cells
312 and immune cells. Coculture with conditioned medium still elevated Cd80 and Cd86 in both
313 groups, with a much higher induction of M2 marker Cd206 in KPP group. Intriguingly, the
314 addition of Cxcl2 in conditioned medium from KP was able to reduce Cd80 and Cd86 while
315 increasing the level of Cd206. Besides, adding CXCR1/CXCR2 inhibitor in conditioned medium
316 from KPP group elevated Cd80 and Cd86 but attenuated Cd206 expression. However, MHC-II
317 was not disturbed by either Cxcl2 or SX-682. Considering that mouse Cxcl2 binds to Cxcr2 with
318 much higher affinity, and mouse Cxcr1 is mainly for Cxcl6 [46], the off-target effect of SX-682
319 in our experimental setting cannot be ignored. To address this issue, we performed a parallel
320 coculture experiment of BMDM with conditioned medium from KP, and KPP treated with IgG
321 control or anti-Cxcl2 neutralization antibodies (**Figs. 4E-4F**). Treatment with neutralization
322 antibodies witnessed a uptrend of Cd80 and Cd86 but a downtrend of Cd206, with a unchanged
323 status of MHC-II, reassuring the results obtained from SX-682. These data illustrated that Cxcl2
324 was partially responsible for the effect of PLK1 in suppressing antigen presentation and inducing
325 M2 polarization. As costimulatory factors in professional antigen presentation cells, the functions

326 of CD80 and CD86 were similar in dendritic cells, and CD206 was also a hallmark of immature
327 dendritic cells [48]. Thus, detection of these markers in dendritic cells has similar value in
328 dissecting the biological effect of PLK1 and CXCL2. To further determine the effect of PLK1 and
329 CXCL2 on antigen presentation, we repeated all three coculture experiments with dendritic cells
330 isolated from bone marrow. The results revealed that alternations of Cd80, Cd86 and Cd206 were
331 quite similar and repeatable, but the level of MHC-II displayed distinct changes. In coculture
332 experiment with KP or KPP cells, increased proportion of KP cells accompanied elevated level of
333 MHC-II, but increased ratio of KPP cell reduced MHC-II expression (**Figs. S5A-S5B**). This was
334 different from the results in BMDM, where a higher ratio of both cell lines was associated with a
335 lower level of MHC-II. However, in both settings, KPP cells were capable of diminishing MHC-
336 II expression more strongly compared to KP, suggesting a universal suppression of antigen
337 presentation. On the other hand, the effect of Cxcl2 on MHC-II was highly in congruent with PLK1,
338 as treatment with Cxcl2 in KP group reduced MHC-II expression and treatment with either SX-
339 682 or neutralization antibodies in KPP group elevated MHC-II level (**Figs. S5C-S5F**). Taken
340 together, these results stated that CXCL2 accounted for the immunosuppressive function of PLK1
341 in LUAD, but the actual effect of CXCL2 might vary in different immune cells.

342

343 **PLK1 negatively regulates MHC-II in cancer cells.**

344 It has been reported that MHC-II can also express on the surface of cancer cells, and this phenotype
345 is associated with improved response to immunotherapy and better survival of cancer patients [49-
346 52]. However, this phenotype was unexplored in lung cancer. Based on these established facts and
347 our observations that PLK1 negatively associated with MHC-II, we aimed to explore whether
348 PLK1 affected expression of MHC-II in LUAD tumors. We first detected MHC-II expression by

349 IHC staining on tumor slides prepared from KP and KPP mice, and the results indeed showed that
350 both tumors expressed MHC-II, with more striking expression in KPP tumors (**Fig. 5A**). This was
351 consistent with the results observed in immune cells that high PLK1 led to lower MHC-II level.
352 Next, we performed flow cytometry analysis of MHC-II level in KP and KPP cell lines, and the
353 results verified the lower expression of MHC-II in KPP cells (**Figs. 5B-5C**). Since MHC-II
354 expression in cancer cells depends on the interferon gamma (IFN-γ) [53], we performed ELISA
355 experiment to detect intracellular IFN-γ amounts between KP and KPP cells. As expected, KPP
356 cells had a lower level of IFN-γ compared to KP (**Fig. 5D**), consistent with its inferior expression
357 of MHC-II. To direct assess the effect of PLK1, we treated KP and KPP with three PLK1 inhibitors
358 (PLKi), including BI-2536 (BI), GSK461364A (GSK) and Onvansertib (ONV). In both cells,
359 treatment with PLK1i consistently elevated the level of MHC-II (**Figs. 5E-5H**), confirming the
360 negative regulation of MHC-II by PLK1. To assess the human side, we utilized human H358
361 LUAD cell line to see whether PLK1 played a similar role. We first transfected H358 cells with
362 siRNA targeting PLK1, and the depletion of PLK1 elevated MHC-II as expected (**Figs. 5I-5J**).
363 Dose escalation of PLKi showed a gradual increase in MHC-II expression (**Figs. 5K-5L**),
364 reassuring the effect of PLK1. Cumulatively, these data supported the conclusion that PLK1 also
365 regulated MHC-II in LUAD cancer cells.

366

367 **Clinical assessment of PLK1 negatively regulating MHC-II**

368 We've previously demonstrated that high PLK1 was associated with worse patients' outcomes
369 [20], and this was consistent with the data that PLK1 suppressing MHC-II in immune cells and
370 cancer cells presented in this study. To evaluate the translational values of our findings, we
371 analyzed the TCGA-LUAD dataset. We first classified all patients into high PLK1 and low PLK1

372 groups based on the median expression of PLK1. We found that high PLK1 was associated with a
373 general low levels of MHC-II member genes (**Fig. 6A**). Using this MHC-II genes signature, we
374 calculated the MHC-II signature scores of all patients and used these signature scores to re-classify
375 patients into high MHC-II high and low MHC-II groups, then performed survival analysis of those
376 patients. We found that patients with high MHC-II scores had better survival outcomes compared
377 to patients with low MHC-II scores (**Fig. 6B**). Given that MHC-II was negatively regulated by
378 PLK1, and low PLK1 was also an indicator of better survival, these results were consistent with
379 our previous findings and further demonstrated that PLK1 promoted LUAD progression. In
380 conclusion, PLK1 was negatively associated with MHC-II in clinical situations, and this affected
381 patients' survival and might lead to immune suppression in TME, possibly through suppressing
382 antigen presentation pathways in immune cells.

383

384 **Discussion**

385 Here in this study, we render pioneering data to support the fact that PLK1 promoted an
386 immunosuppressive TME in LUAD (**Fig. 7**). Under low PLK1 condition, TME is characterized
387 by a higher proportion of tumor infiltrating immune cells and lower level of CXCL2, and this
388 condition is associated with more M1 polarization and functional antigen presentation pathway. In
389 addition, tumors express more MHC-II and this feature is associated with better patient's survival.
390 Under high PLK1 condition, TME is characterized by low tumor infiltrating immune cells and
391 high secreted CXCL2, which promotes M2 polarization and disrupts antigen processing and
392 presentation. Tumors in this situation also express a lower level of MHC-II, which is associated
393 with worse outcomes of patients. The differences in TME shown in high PLK1 and low PLK1

394 conditions suggest that PLK1 is an important modulator of TME, and targeting PLK1 may be a
395 practical therapeutic intervention in LUAD treatment.

396 Survival of lung cancer is suboptimal due to limitation of diagnosis and treatment, with 60% five-
397 year survival rate for localized diseases, which further drops to less than 5% for metastatic cancer
398 [1]. Although the emergence of immunotherapy has expanded the treatment options for lung
399 cancer patients, the efficacy is questionable due resistance to immunotherapy [54, 55]. Thus,
400 identifying mechanisms behind this harmful condition is urgently needed. Here, we report a novel
401 mechanism of PLK1 in cancer promotion. We show that PLK1 induces an immunosuppressive
402 TME in LUAD by undermining M1 polarization and antigen presentation, which negatively
403 impacts anti-tumor immunity in LUAD. PLK1 has been largely considered as a canonical cell
404 cycle regulator in the past decades. However, recent studies have gradually uncovered the tumor-
405 promoting functions of this kinase. Clearly, PLK1 is involved in multiple hallmarks of cancer, and
406 targeting PLK1 has potential to control disease progression [56]. Specifically in LUAD, we've
407 demonstrated that PLK1 promotes LUAD progression via phosphorylation of receptor tyrosine
408 kinase RET, which activates MAPK cascade and leads to proliferation and progression [20].
409 Together with the data in this study, PLK1 may be a critical modulator involving multiple cancer
410 hallmarks of LUAD. Future studies will discover more innovative functions of PLK1 in cancer
411 progression.

412 The fact that PLK1 suppresses anti-tumor in LUAD is intriguing given that immunotherapy is one
413 of the major therapeutic approaches for lung cancer. The major reasons of resistance to
414 immunotherapies are the scarcity of tumor-infiltrating immune cells and existence of immune
415 checkpoints [57]. We show that high PLK1 is associated with lower infiltrating cytotoxic T cells,
416 and this feature is harmful to anti-tumor response in LUAD. The decreased infiltration of T cells

417 may be due to the increased M2 polarization from TAM, which is a well-established suppressor
418 of T cells functions. Besides, functional antigen presentation in TME is the key to the success of
419 anti-tumor immune response, and immune evasion through suppressing this critical process
420 significantly reduces the efficacy of immunotherapy [39]. The novelty of our study lies in the fact
421 we first demonstrate that PLK1 inhibits antigen presentation pathway by down regulating MHC-
422 II in M2 macrophages, which is the key molecule responsible for processing and presentation of
423 tumor-specific neoantigens. Besides, this conclusion can be extended to cancer cells, where high
424 PLK1 is also associated with low MHC-II expression. The expression of MHC-II in tumors is a
425 good biomarker for better survival of patients [49-52]. However, the function of MHC-II in cancer
426 cells is unclear. Given that MHC-II is mainly responsible for antigen presentation by professional
427 APC, the fact that MHC-II expressing in cancer cells may be involved in this process by
428 functionally mimicking antigen presentation process and priming CD4 T cells, which directly bind
429 to MHC-II to activate immune response, and this idea has been supported by the discovery of
430 certain MHC-II specific neoantigens in tumor cells and their necessity in promoting successful
431 anti-tumor response [52]. Considering the negative regulation of MHC-II by PLK1, our study
432 further supports this notion in LUAD. However, the mechanistic part behind this regulation is
433 missing and requires further exploration.

434 Considering the predominant immunosuppressive functions of PLK1 in LUAD and other cancer
435 types [21, 22], treatment focuses on targeting PLK1 may decelerate tumor growth by boosting
436 immune response in TME. However, it is noteworthy that PLK1 may be negatively correlated with
437 PD-L1 in certain situations [21, 22], devaluing the monotherapy with PLK1 inhibitor as this
438 approach will unexpectedly elevate immune checkpoints. Thus, combination treatment with PLKi

439 and immune checkpoints blockade should exhibit premium effect, and this assumption remains to
440 be investigated by future studies.

441

442 **Acknowledgement**

443 This study is supported by NIH R01 CA157429 (XL), R01 CA196634 (XL), R01 CA264652 (XL),
444 R01 CA256893 (XL). This study is also supported by the Biospecimen Procurement &
445 Translational Pathology, Biostatistics and Bioinformatics, Redox Metabolism, Flow Cytometry
446 and Immune Monitoring Shared Resources, and OncoGenomics Shared Resource Facility of the
447 University of Kentucky Markey Cancer Center (P30CA177558).

448

449 **Data availability**

450 All data are included in this article and the original data are available from the corresponding
451 author upon reasonable request. Bulky RNA-seq data was deposited in GEO under accession
452 number GSE206644.

453

454

455

456

457

458

459 **Figure 1. Single-cell RNA-seq analysis of KP and KPP mice.**

460 **A,** Workflow of single-cell RNA-seq of LSL-Kras^{G12D}/Tp53$^{f/f}$ (KP) and LSL-
461 Kras^{G12D}/Tp53$^{f/f}$/LSL-Plk1 (KPP) mice. Ad-Cre, adenovirus-expressing Cre recombinase. **B,**
462 UMAP projection of major immune cell populations in KP and KPP groups. **C,** Comparison of
463 cell populations denoted in B between KP and KPP (n=3). **D,** Proportion of cell populations in KP
464 and KPP. *, $p < 0.05$. **, $p < 0.01$. ***, $p < 0.001$.

465

466

467

468

469

470

471

472

473

474

475

476

477

478 **Figure 2. High PLK1 is associated with M2-predominant phenotype.**

479 **A,** Volcano plot of differentially expressed genes (KPP vs KP, FDR < 0.05) in macrophages. Top
480 10 up and down regulated genes (ranked by Log2FC) are labeled. Log10FDR, Log10-transformed
481 FDR. Log2FC, Log2-transformed fold change (FC). **B,** Top 10 up and down regulated genes
482 identified in A. **C,** Expression (KPP vs KP) of canonical M1 markers (Il1b, Tlr2, Cd86, Cd68,
483 Cd80, Socs3, Gch1) and M2 markers (Fn1, Pparg, Arg1, Slco2b1, Ptgs1, Pygl, Cd206). **D,**
484 Representative genes and functional markers used for identification of M1 (Cd38, Fcgr1) and M2
485 (Marco, Pparg). **E,** UMAP of M1 and M2 macrophages identified based on D. **F,** Proportion of
486 M1 and M2 in KP and KPP.

487

488

489

490

491

492

493

494

495

496

497

498 **Figure 3. PLK1 suppresses antigen presentation pathway and promotes M2 polarization.**

499 **A,** Significant up and down regulated pathways (KPP vs KP, FDR < 0.1) in macrophages identified
500 by GSEA. NES, normalized enrichment score. **B,** GSEA plots of three exemplary pathways in A.
501 **C,** Flow cytometry analysis of indicated genes in BMDM cocultured with KP or KPP at the
502 indicated ratio for 48h. **D,** Quantification of C (n=3). *, $p < 0.05$. ***, $p < 0.001$.

503

504

505

506

507

508

509

510

511

512

513

514

515

516

517 **Figure 4. CXCL2 is responsible for the immunosuppressive function of PLK1.**

518 **A,** Cytokines array detection of cytokines secretion from culture medium between KP and KPP.
519 Visible differences are labeled. **B,** Illustration of CXCL2's function in suppressing anti-tumor
520 immunity. **C,** Flow cytometry analysis of BMDM cocultured with conditioned medium from KP
521 or KPP for 48h, with or without recombinant Cxcl2 (2ug/ml) or CXCR1/CXCR2 inhibitor SX-682
522 (1μM) treatment. **D,** Quantification of C (n=3). **E,** Flow cytometry analysis of BMDM cocultured
523 with conditioned medium from KP or KPP for 48h, with or without anti-Cxcl2 neutralization
524 antibodies (5ug/ml) treatment. **F,** Quantification of E (n=3). *, $p < 0.05$. **, $p < 0.01$. ***, $p <$
525 0.001.

526

527

528

529

530

531

532

533

534

535

536

537 **Figure 5. PLK1 suppresses MHC-II expression in tumor cells.**

538 **A,** Representative IHC images of KP and KPP tumors stained with MHC-II antibodies. **B,** Flow
539 cytometry detection of MHC-II in KP and KPP cells. **C,** Quantification of B (n=3). Data are
540 normalized to KP and shown as mean±SD. **D,** ELISA detection of IFN-γ in KP and KPP cells
541 (n=6). Data are normalized to KP and shown as mean±SD. **E,** Flow cytometry detection of MHC-
542 II in KP cells treated with PLK1 inhibitors (50nM BI, 50nM GSK, 200nM ONV) for 48h. **F,**
543 Quantification of E (n=3). Data are normalized to Ctrl and shown as mean±SD. **G,** Flow cytometry
544 detection of MHC-II in KPP cells treated with PLK1 inhibitors (50nM BI, 50nM GSK, 200nM
545 ONV) for 48h. **H,** Quantification of G (n=3). Data are normalized to Ctrl and shown as mean±SD.
546 For these results, an unpaired one-sided t test was used. **I,** Flow cytometry detection of MHC-II in
547 H358 cells 48h after transfection with siRNA control or siRNA targeting PLK1. **J,** Quantification
548 of I (n=3). Data are normalized to Ctrl and shown as mean±SD. **K,** Flow cytometry detection of
549 MHC-II in H358 cells with dose escalation of PLK1 inhibitor ONV (nM) for 48h. **L,**
550 Quantification of K (n=3). Data are normalized to untreated group (0) and shown as mean±SD. *,
551 $p < 0.05$. **, $p < 0.01$. ***, $p < 0.001$.

552

553

554

555

556

557

558 **Figure 6. Clinical evidence of PLK1 suppressing MHC-II in lung cancer.**

559 **A,** Heatmap of MHC-II signature genes in TCGA-LUAD patients separated into PLK1 high and
560 PLK1 low groups. Data (zscore) of PLK1 and MHC-II genes are used. Patients are clustered based
561 on the median value of PLK1. **B,** Survival curves of TCGA-LUAD patients separated into MHC-
562 II high and MHC-II low groups. Data (RSEM) of MHC-II signature genes in A are first Log2+1-
563 transformed, then averaged to get signature scores. Patients are clustered based on the median
564 value of signature scores. For these results, a log-rank test was used.

565

566

567

568

569

570

571

572

573

574

575

576

577 **Figure 7. Summary of working model.**

578 Under low PLK1 condition, there is low level of CXCL2 secreted from tumors. Tumor
579 microenvironment is "hot", characterized by increased tumor infiltrating immune cells, M1
580 polarization of TAM and functional APC. Cancer cells are MHC-II high and this feature is
581 associated with better survival of patients. Under high PLK1 condition, there is increased secretion
582 of CXCL2 from tumors. Tumor microenvironment is "cold", characterized by low levels of tumor
583 infiltrating immune cells, M2 polarization of TAM and dysfunctional APC. Cancer cells are MHC-
584 II low and patients have worse survival outcomes.

585

586

587

588

589

590

591

592

593

594

595

596

597 **Figure S1. Single-cell RNA-seq analysis.**

598 **A,** UMAP projection of all cells in single-cell RNA-seq undergoing unsupervised clustering. **B,**
599 Heatmap of signature genes of each cluster in A. **C,** Proportion of each cluster in KP and KPP. **D,**
600 Comparison of clusters between KP and KPP. For these results, a Wilcoxon rank-sum test was
601 used. **E,** Representative genes used for supervised clustering of major immune cell populations in
602 Fig. 1A. ***, FDR < 0.001.

603

604

605

606

607

608

609

610

611

612

613

614

615

616 **Figure S2. Single-cell RNA-seq analysis of T cell populations.**

617 **A,** Representative genes used for supervised clustering of T cell populations. **B,** UMAP projection
618 of T cell populations based on features genes in A. **C,** Comparison of T cell populations denoted
619 in B between KP and KPP (n=3). **D,** Proportion of T cell populations in KP and KPP. *, $p < 0.05$.
620 **, $p < 0.01$. ***, $p < 0.001$.

621

622

623

624

625

626

627

628

629

630

631

632

633

634

635 **Figure S3. GSEA results of immune cell populations.**

636 Significant up and down regulated pathways (KPP vs KP, FDR < 0.1) in major immune cell
637 populations except macrophages are shown. NES, normalized enrichment score.

638

639

640

641

642

643

644

645

646

647

648

649

650

651

652

653

654 **Figure S4. RNA-seq analysis of KP and KPP cells.**

655 **A,** STRING analysis of functional genes associated with CXCL2 in human and mice. **B,** GSEA
656 table of two potential pathways regulating CXCL2 secretion in KPP cells, identified by our
657 previously published RNA-seq data (GSE206644, KPP vs KP). FDR < 0.05 indicates a
658 significance.

659

660

661

662

663

664

665

666

667

668

669

670

671

672

673 **Figure S5. Coculture experiments of dendritic cells.**

674 **A,** Flow cytometry analysis of indicated genes in dendritic cells cocultured with KP or KPP at the
675 indicated ratio for 48h. **B,** Quantification of A (n=3). **C,** Flow cytometry analysis of dendritic cells
676 cocultured with conditioned medium from KP or KPP for 48h, with or without recombinant Cxcl2
677 (2ug/ml) or CXCR1/CXCR2 inhibitor SX-682 (1μM) treatment. **D,** Quantification of C (n=3). **E,**
678 Flow cytometry analysis of dendritic cells cocultured with conditioned medium from KP or KPP,
679 with or without anti-Cxcl2 neutralization antibodies (5ug/ml) treatment. **F,** Quantification of E
680 (n=3). *, $p < 0.05$. **, $p < 0.01$. ***, $p < 0.001$.

681

682

683

684

685

686

687

688

689

690

691

692

693 **Figure S6. Correlation analysis of PLK1 and MHC-II genes.**

694 Patients' data are collected from TCGA-LUAD. Data (RSEM) of PLK1 and MHC-II genes are
695 Log2-transformed. r_s, spearman coefficient.

696

697

698

699

700

701

702

703

704

705

706

707

708

709

710

711

712 **Reference**

713 1. Siegel, R.L., et al., *Cancer statistics, 2023.* CA Cancer J Clin, 2023. **73**(1): p. 17-48.

714 2. Travis, W.D., et al., *International association for the study of lung cancer/american*
715 *thoracic society/european respiratory society international multidisciplinary classification*
716 *of lung adenocarcinoma.* J Thorac Oncol, 2011. **6**(2): p. 244-85.

717 3. Devarakonda, S., D. Morgensztern, and R. Govindan, *Genomic alterations in lung*
718 *adenocarcinoma.* Lancet Oncol, 2015. **16**(7): p. e342-51.

719 4. Doroshow, D.B., et al., *Immunotherapy in Non-Small Cell Lung Cancer: Facts and Hopes.*
720 Clin Cancer Res, 2019. **25**(15): p. 4592-4602.

721 5. Altorki, N.K., et al., *The lung microenvironment: an important regulator of tumour growth*
722 *and metastasis.* Nat Rev Cancer, 2019. **19**(1): p. 9-31.

723 6. Sharma, P. and J.P. Allison, *Immune checkpoint targeting in cancer therapy: toward*
724 *combination strategies with curative potential.* Cell, 2015. **161**(2): p. 205-14.

725 7. Zappasodi, R., T. Merghoub, and J.D. Wolchok, *Emerging Concepts for Immune*
726 *Checkpoint Blockade-Based Combination Therapies.* Cancer Cell, 2018. **33**(4): p. 581-598.

727 8. Hellmann, M.D., et al., *Nivolumab plus Ipilimumab in Lung Cancer with a High Tumor*
728 *Mutational Burden.* N Engl J Med, 2018. **378**(22): p. 2093-2104.

729 9. Gandhi, L., et al., *Pembrolizumab plus Chemotherapy in Metastatic Non-Small-Cell Lung*
730 *Cancer.* N Engl J Med, 2018. **378**(22): p. 2078-2092.

731 10. Seki, A., et al., *Bora and the kinase Aurora a cooperatively activate the kinase Plk1 and*
732 *control mitotic entry.* Science, 2008. **320**(5883): p. 1655-8.

733 11. Golsteyn, R.M., et al., *Cell cycle regulation of the activity and subcellular localization of*
734 *Plk1, a human protein kinase implicated in mitotic spindle function.* J Cell Biol, 1995.
735 **129**(6): p. 1617-28.
736 12. Elowe, S., et al., *Tension-sensitive Plk1 phosphorylation on BubR1 regulates the stability*
737 *of kinetochore microtubule interactions.* Genes Dev, 2007. **21**(17): p. 2205-19.
738 13. Lane, H.A. and E.A. Nigg, *Antibody microinjection reveals an essential role for human*
739 *polo-like kinase 1 (Plk1) in the functional maturation of mitotic centrosomes.* J Cell Biol,
740 1996. **135**(6 Pt 2): p. 1701-13.
741 14. Neef, R., et al., *Phosphorylation of mitotic kinesin-like protein 2 by polo-like kinase 1 is*
742 *required for cytokinesis.* J Cell Biol, 2003. **162**(5): p. 863-75.
743 15. Schmidt, A., et al., *Xenopus polo-like kinase Plx1 regulates XErp1, a novel inhibitor of*
744 *APC/C activity.* Genes Dev, 2005. **19**(4): p. 502-13.
745 16. Liu, X.S., B. Song, and X. Liu, *The substrates of Plk1, beyond the functions in mitosis.*
746 Protein Cell, 2010. **1**(11): p. 999-1010.
747 17. Strebhardt, K. and A. Ullrich, *Targeting polo-like kinase 1 for cancer therapy.* Nat Rev
748 Cancer, 2006. **6**(4): p. 321-30.
749 18. Gutteridge, R.E., et al., *Plk1 Inhibitors in Cancer Therapy: From Laboratory to Clinics.*
750 Mol Cancer Ther, 2016. **15**(7): p. 1427-35.
751 19. Shin, S.B., et al., *Active PLK1-driven metastasis is amplified by TGF-β signaling that forms*
752 *a positive feedback loop in non-small cell lung cancer.* Oncogene, 2020. **39**(4): p. 767-785.
753 20. Kong, Y., et al., *The kinase PLK1 promotes the development of Kras/Tp53-mutant lung*
754 *adenocarcinoma through transcriptional activation of the receptor RET.* Sci Signal, 2022.
755 **15**(754): p. eabj4009.

756 21. Reda, M., et al., *Development of a nanoparticle-based immunotherapy targeting PD-L1*
757 *and PLK1 for lung cancer treatment.* Nat Commun, 2022. **13**(1): p. 4261.
758 22. Zhang, Z., et al., *Targeting Plk1 Sensitizes Pancreatic Cancer to Immune Checkpoint*
759 *Therapy.* Cancer Res, 2022. **82**(19): p. 3532-3548.
760 23. DuPage, M., A.L. Dooley, and T. Jacks, *Conditional mouse lung cancer models using*
761 *adenoviral or lentiviral delivery of Cre recombinase.* Nat Protoc, 2009. **4**(7): p. 1064-72.
762 24. McGinnis, C.S., L.M. Murrow, and Z.J. Gartner, *DoubletFinder: Doublet Detection in*
763 *Single-Cell RNA Sequencing Data Using Artificial Nearest Neighbors.* Cell Syst, 2019.
764 **8**(4): p. 329-337.e4.
765 25. Stuart, T., et al., *Comprehensive Integration of Single-Cell Data.* Cell, 2019. **177**(7): p.
766 1888-1902.e21.
767 26. Korsunsky, I., et al., *Fast, sensitive and accurate integration of single-cell data with*
768 *Harmony.* Nat Methods, 2019. **16**(12): p. 1289-1296.
769 27. Love, M.I., W. Huber, and S. Anders, *Moderated estimation of fold change and dispersion*
770 *for RNA-seq data with DESeq2.* Genome Biol, 2014. **15**(12): p. 550.
771 28. Gennady, K., et al., *Fast gene set enrichment analysis.* bioRxiv, 2021: p. 060012.
772 29. Liberzon, A., et al., *The Molecular Signatures Database (MSigDB) hallmark gene set*
773 *collection.* Cell Syst, 2015. **1**(6): p. 417-425.
774 30. Kanehisa, M. and S. Goto, *KEGG: kyoto encyclopedia of genes and genomes.* Nucleic
775 Acids Res, 2000. **28**(1): p. 27-30.
776 31. Szklarczyk, D., et al., *The STRING database in 2023: protein-protein association networks*
777 *and functional enrichment analyses for any sequenced genome of interest.* Nucleic Acids
778 Res, 2023. **51**(D1): p. D638-d646.

779 32. Gao, J., et al., *Integrative analysis of complex cancer genomics and clinical profiles using*
780 *the cBioPortal.* Sci Signal, 2013. **6**(269): p. pl1.
781 33. Cerami, E., et al., *The cBio cancer genomics portal: an open platform for exploring*
782 *multidimensional cancer genomics data.* Cancer Discov, 2012. **2**(5): p. 401-4.
783 34. *Comprehensive molecular profiling of lung adenocarcinoma.* Nature, 2014. **511**(7511): p.
784 543-50.
785 35. Yu, T., et al., *Modulation of M2 macrophage polarization by the crosstalk between Stat6*
786 *and Trim24.* Nat Commun, 2019. **10**(1): p. 4353.
787 36. Lin, Y., J. Xu, and H. Lan, *Tumor-associated macrophages in tumor metastasis: biological*
788 *roles and clinical therapeutic applications.* J Hematol Oncol, 2019. **12**(1): p. 76.
789 37. Cain, D.W. and J.A. Cidlowski, *Immune regulation by glucocorticoids.* Nat Rev Immunol,
790 2017. **17**(4): p. 233-247.
791 38. Roche, P.A. and K. Furuta, *The ins and outs of MHC class II-mediated antigen processing*
792 *and presentation.* Nat Rev Immunol, 2015. **15**(4): p. 203-16.
793 39. Jhunjhunwala, S., C. Hammer, and L. Delamarre, *Antigen presentation in cancer: insights*
794 *into tumour immunogenicity and immune evasion.* Nat Rev Cancer, 2021. **21**(5): p. 298-
795 312.
796 40. de Visser, K.E. and J.A. Joyce, *The evolving tumor microenvironment: From cancer*
797 *initiation to metastatic outgrowth.* Cancer Cell, 2023. **41**(3): p. 374-403.
798 41. Mauer, J., et al., *Signaling by IL-6 promotes alternative activation of macrophages to limit*
799 *endotoxemia and obesity-associated resistance to insulin.* Nat Immunol, 2014. **15**(5): p.
800 423-30.

801 42. Wolpe, S.D., et al., *Macrophages secrete a novel heparin-binding protein with*
802 *inflammatory and neutrophil chemokinetic properties.* J Exp Med, 1988. **167**(2): p. 570-
803 81.
804 43. Murooka, T.T., et al., *CCL5-mediated T-cell chemotaxis involves the initiation of mRNA*
805 *translation through mTOR/4E-BP1.* Blood, 2008. **111**(10): p. 4892-901.
806 44. Zhang, H., et al., *CXCL2/MIF-CXCR2 signaling promotes the recruitment of myeloid-*
807 *derived suppressor cells and is correlated with prognosis in bladder cancer.* Oncogene,
808 2017. **36**(15): p. 2095-2104.
809 45. Hu, J., et al., *Regulation of tumor immune suppression and cancer cell survival by*
810 *CXCL1/2 elevation in glioblastoma multiforme.* Sci Adv, 2021. **7**(5).
811 46. Fan, X., et al., *Murine CXCR1 is a functional receptor for GCP-2/CXCL6 and interleukin-*
812 *8/CXCL8.* J Biol Chem, 2007. **282**(16): p. 11658-66.
813 47. Greene, S., et al., *Inhibition of MDSC Trafficking with SX-682, a CXCR1/2 Inhibitor,*
814 *Enhances NK-Cell Immunotherapy in Head and Neck Cancer Models.* Clin Cancer Res,
815 2020. **26**(6): p. 1420-1431.
816 48. Wollenberg, A., et al., *Expression and function of the mannose receptor CD206 on*
817 *epidermal dendritic cells in inflammatory skin diseases.* J Invest Dermatol, 2002. **118**(2):
818 p. 327-34.
819 49. Johnson, D.B., et al., *Melanoma-specific MHC-II expression represents a tumour-*
820 *autonomous phenotype and predicts response to anti-PD-1/PD-L1 therapy.* Nat Commun,
821 2016. **7**: p. 10582.
822 50. Rodig, S.J., et al., *MHC proteins confer differential sensitivity to CTLA-4 and PD-1*
823 *blockade in untreated metastatic melanoma.* Sci Transl Med, 2018. **10**(450).

824 51. Roemer, M.G.M., et al., *Major Histocompatibility Complex Class II and Programmed*
825 *Death Ligand 1 Expression Predict Outcome After Programmed Death 1 Blockade in*
826 *Classic Hodgkin Lymphoma.* J Clin Oncol, 2018. **36**(10): p. 942-950.
827 52. Alspach, E., et al., *MHC-II neoantigens shape tumour immunity and response to*
828 *immunotherapy.* Nature, 2019. **574**(7780): p. 696-701.
829 53. Axelrod, M.L., et al., *Biological Consequences of MHC-II Expression by Tumor Cells in*
830 *Cancer.* Clin Cancer Res, 2019. **25**(8): p. 2392-2402.
831 54. Sharma, P., et al., *Primary, Adaptive, and Acquired Resistance to Cancer Immunotherapy.*
832 Cell, 2017. **168**(4): p. 707-723.
833 55. O'Donnell, J.S., M.W.L. Teng, and M.J. Smyth, *Cancer immunoediting and resistance to*
834 *T cell-based immunotherapy.* Nat Rev Clin Oncol, 2019. **16**(3): p. 151-167.
835 56. Lee, K.S., et al., *Recent Advances and New Strategies in Targeting Plk1 for Anticancer*
836 *Therapy.* Trends Pharmacol Sci, 2015. **36**(12): p. 858-877.
837 57. Restifo, N.P., M.J. Smyth, and A. Snyder, *Acquired resistance to immunotherapy and*
838 *future challenges.* Nat Rev Cancer, 2016. **16**(2): p. 121-6.

839

Figure 1

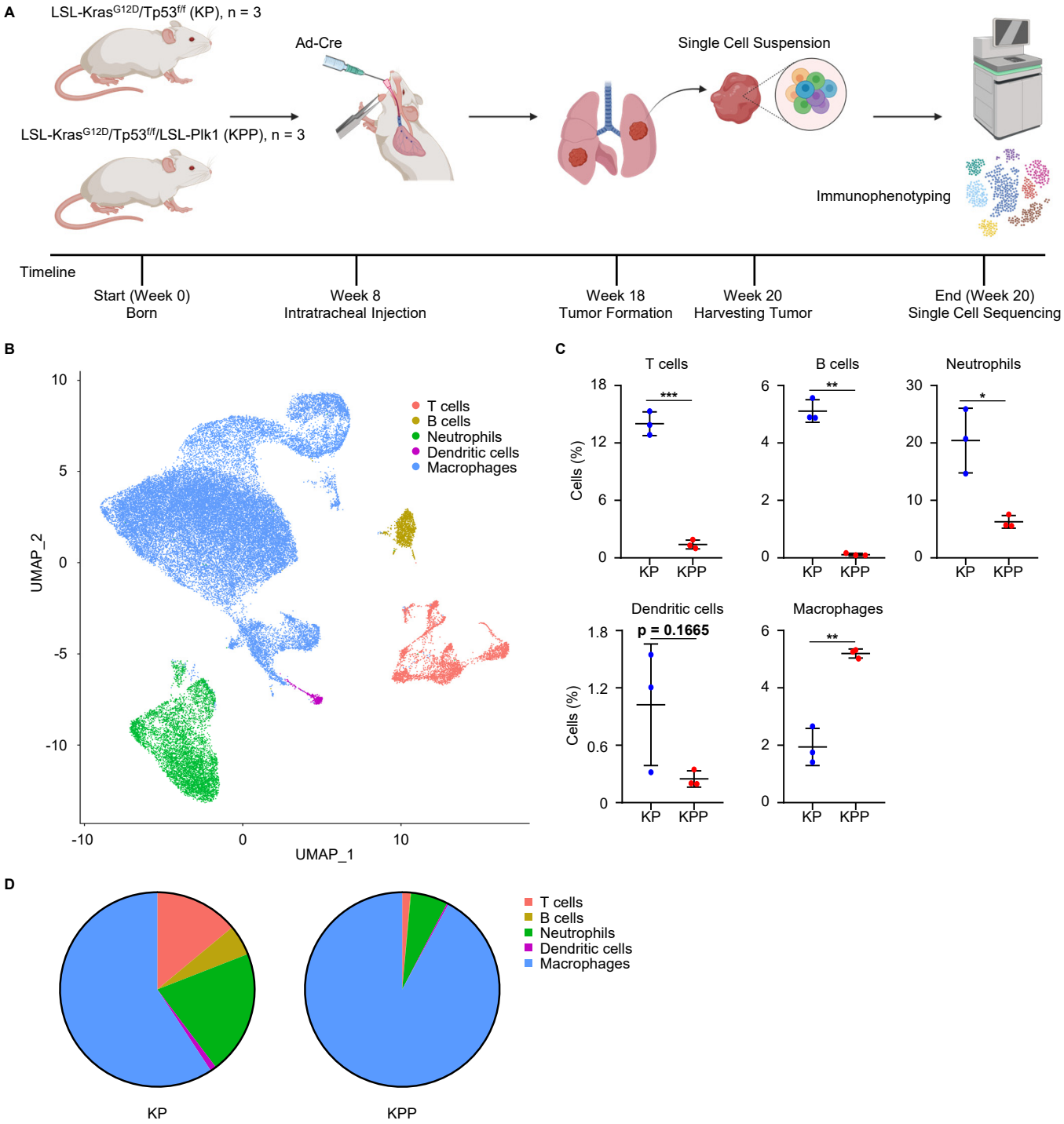
A
LSL-Kras^{G12D}/Tp53$^{f/f}$ (KP), n = 3
LSL-Kras^{G12D}/Tp53$^{f/f}$/LSL-Plk1 (KPP), n = 3
Ad-Cre
Single Cell Suspension
Immunophenotyping
Timeline
Start (Week 0)
Born
Week 8
Intratracheal Injection
Week 18
Tumor Formation
Week 20
Harvesting Tumor
End (Week 20)
Single Cell Sequencing
B
T cells
B cells
Neutrophils
Dendritic cells
Macrophages
UMAP_2
UMAP_1
C
T cells
B cells
Neutrophils
Dendritic cells
Macrophages
Cells (%)
KP
KPP
p = 0.1665
D
T cells
B cells
Neutrophils
Dendritic cells
Macrophages
KP
KPP

Figure 2

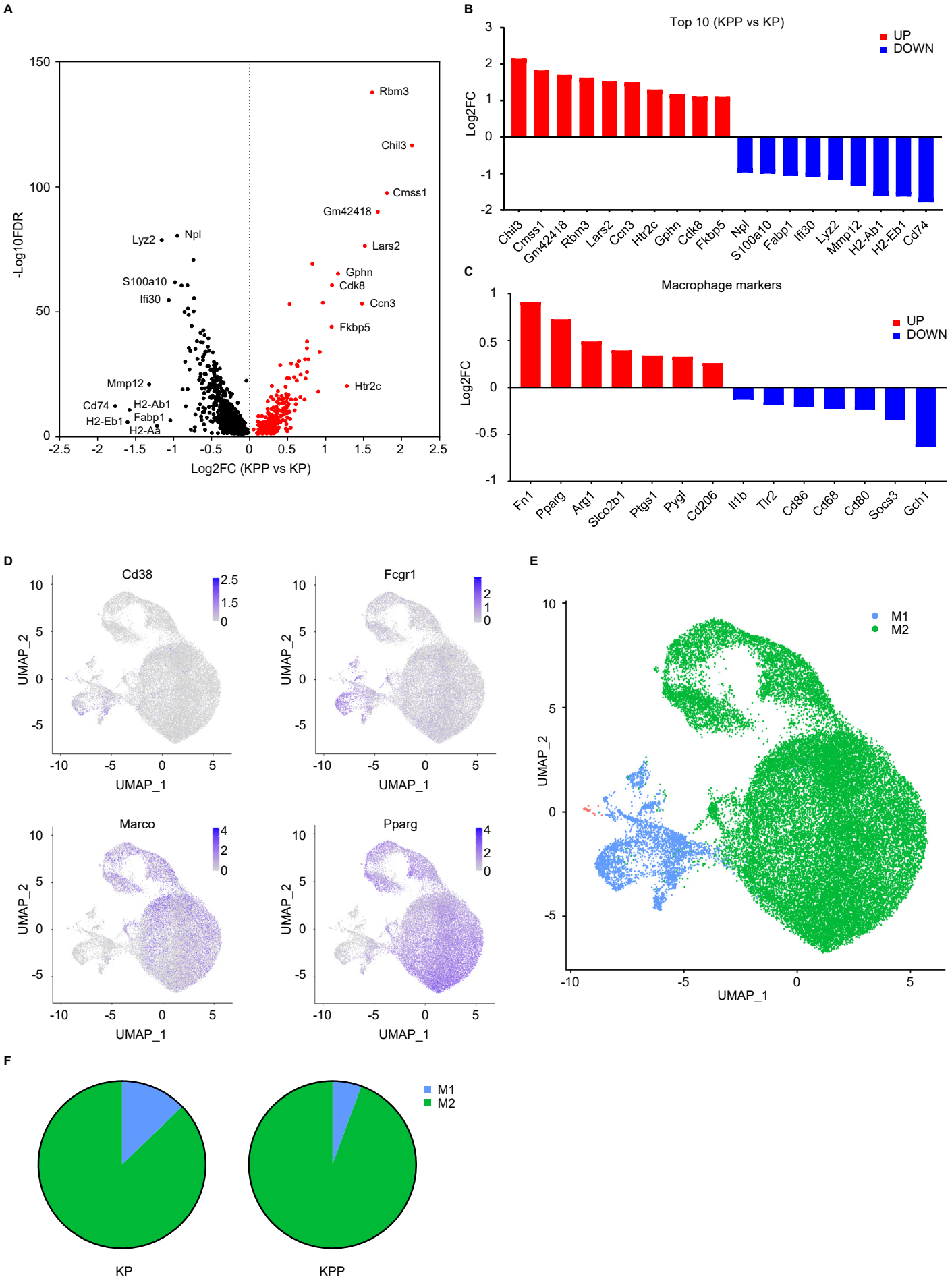
A
-Log10FDR
Log2FC (KPP vs KP)
Rbm3
Chil3
Cmss1
Gm42418
Lars2
Gphn
Cdk8
Ccn3
Fkbp5
Htr2c
Lyz2
Npl
S100a10
Ifi30
Mmp12
Cd74
H2-Ab1
H2-Eb1
Fabp1
H2-Aa
B
Top 10 (KPP vs KP)
UP
DOWN
Log2FC
Chil3
Cmss1
Gm42418
Rbm3
Lars2
Ccn3
Htr2c
Gphn
Cdk8
Fkbp5
Npl
S100a10
Fabp1
Ifi30
Lyz2
Mmp12
H2-Ab1
H2-Eb1
Cd74
C
Macrophage markers
UP
DOWN
Log2FC
Fn1
Pparg
Arg1
Slco2b1
Ptgs1
Pygl
Cd206
Il1b
Tlr2
Cd86
Cd68
Cd80
Socs3
Gch1
D
Cd38
Fcgr1
Marco
Pparg
UMAP_1
UMAP_2
E
M1
M2
UMAP_1
UMAP_2
F
M1
M2
KP
KPP

Figure 3

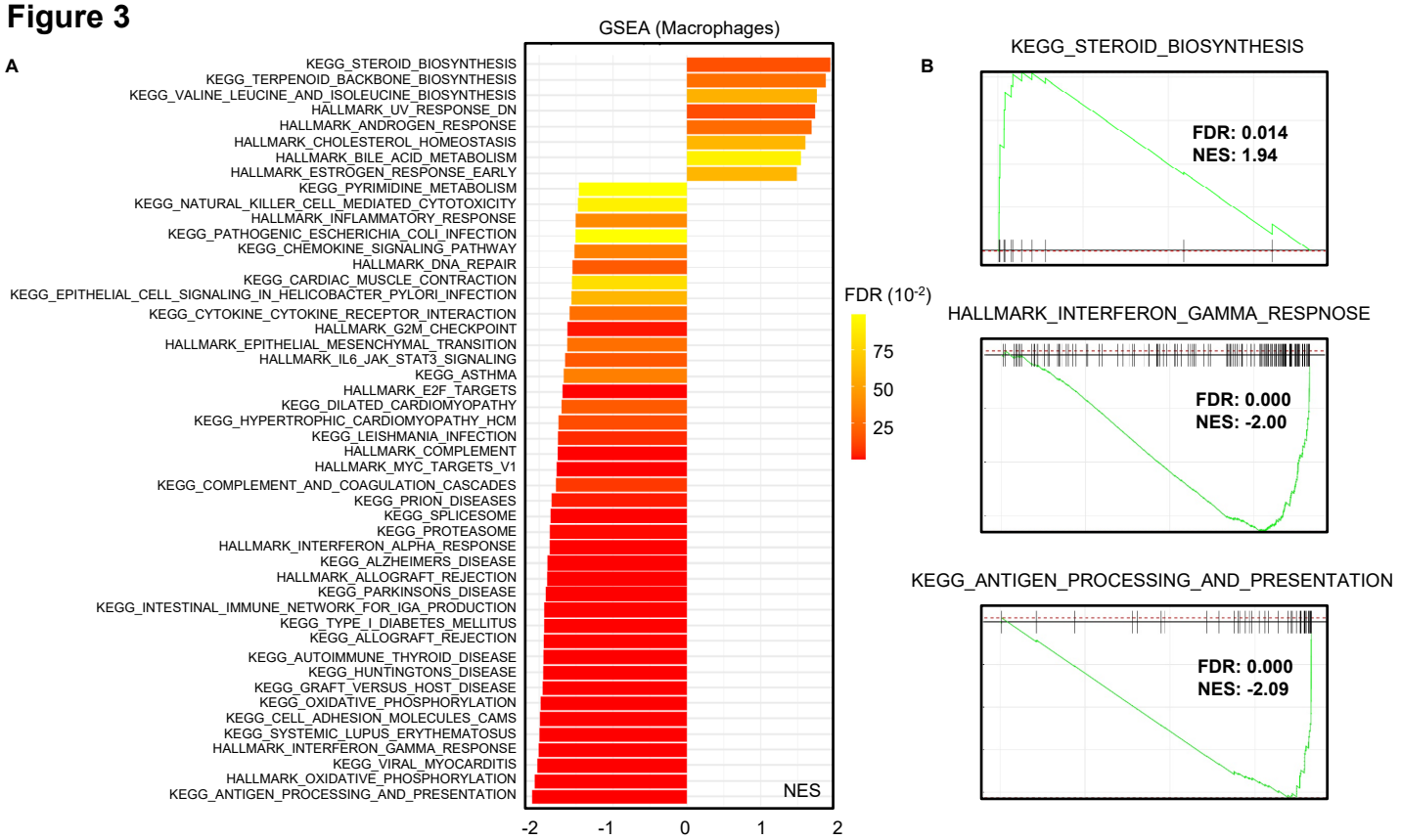
A
GSEA (Macrophages)
KEGG_STEROID_BIOSYNTHESIS
KEGG_TERPENOID_BACKBONE_BIOSYNTHESIS
KEGG_VALINE_LEUCINE_AND_ISOLEUCINE_BIOSYNTHESIS
HALLMARK_UV_RESPONSE_DN
HALLMARK_ANDROGEN_RESPONSE
HALLMARK_CHOLESTEROL_HOMEOSTASIS
HALLMARK_BILE_ACID_METABOLISM
HALLMARK_ESTROGEN_RESPONSE_EARLY
KEGG_PYRIMIDINE_METABOLISM
KEGG_NATURAL_KILLER_CELL_MEDIATED_CYTOTOXICITY
HALLMARK_INFLAMMATORY_RESPONSE
KEGG_PATHOGENIC_ESCHERICHIA_COLI_INFECTION
KEGG_CHEMOKINE_SIGNALING_PATHWAY
HALLMARK_DNA_REPAIR
KEGG_CARDIAC_MUSCLE_CONTRACTION
KEGG_EPITHELIAL_CELL_SIGNALING_IN_HELICOBACTER_PYLORI_INFECTION
KEGG_CYTOKINE_CYTOKINE_RECEPTOR_INTERACTION
HALLMARK_G2M_CHECKPOINT
HALLMARK_EPITHELIAL_MESENCHYMAL_TRANSITION
HALLMARK_IL6_JAK_STAT3_SIGNALING
KEGG_ASTHMA
HALLMARK_E2F_TARGETS
KEGG_DILATED_CARDIOMYOPATHY
KEGG_HYPERTROPHIC_CARDIOMYOPATHY_HCM
KEGG_LEISHMANIA_INFECTION
HALLMARK_COMPLEMENT
HALLMARK_MYC_TARGETS_V1
KEGG_COMPLEMENT_AND_COAGULATION_CASCADES
KEGG_PRION_DISEASES
KEGG_SPLICESOME
KEGG_PROTEASOME
HALLMARK_INTERFERON_ALPHA_RESPONSE
KEGG_ALZHEIMERS_DISEASE
HALLMARK_ALLOGRAFT_REJECTION
KEGG_PARKINSONS_DISEASE
KEGG_INTESTINAL_IMMUNE_NETWORK_FOR_IGA_PRODUCTION
KEGG_TYPE_I_DIABETES_MELLITUS
KEGG_ALLOGRAFT_REJECTION
KEGG_AUTOIMMUNE_THYROID_DISEASE
KEGG_HUNTINGTONS_DISEASE
KEGG_GRAFT_VERSUS_HOST_DISEASE
KEGG_OXIDATIVE_PHOSPHORYLATION
KEGG_CELL_ADHESION_MOLECULES_CAMS
KEGG_SYSTEMIC_LUPUS_ERYTHEMATOSUS
HALLMARK_INTERFERON_GAMMA_RESPONSE
KEGG_VIRAL_MYOCARDITIS
HALLMARK_OXIDATIVE_PHOSPHORYLATION
KEGG_ANTIGEN_PROCESSING_AND_PRESENTATION
NES
-2
-1
0
1
2
FDR (10-2)
75
50
25
B
KEGG_STEROID_BIOSYNTHESIS
FDR: 0.014
NES: 1.94
HALLMARK_INTERFERON_GAMMA_RESPNOSE
FDR: 0.000
NES: -2.00
KEGG_ANTIGEN_PROCESSING_AND_PRESENTATION
FDR: 0.000
NES: -2.09

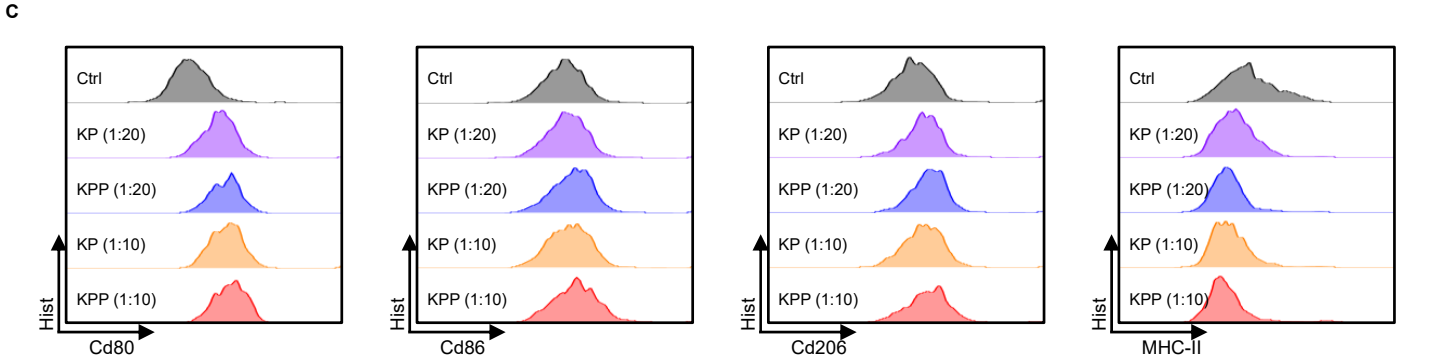
C
Ctrl
KP (1:20)
KPP (1:20)
KP (1:10)
KPP (1:10)
Hist
Cd80
Cd86
Cd206
MHC-II

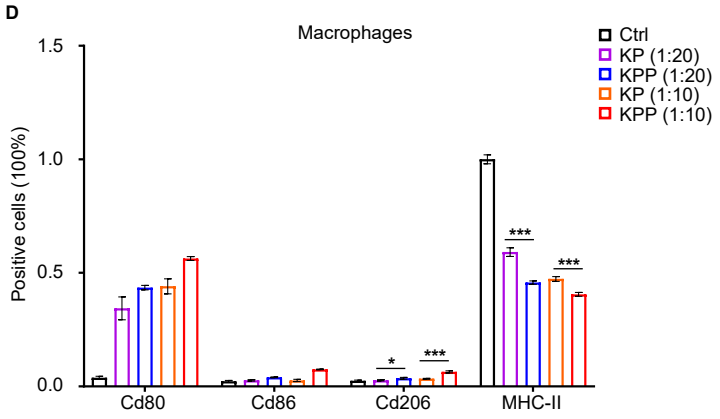
D
Macrophages
Ctrl
KP (1:20)
KPP (1:20)
KP (1:10)
KPP (1:10)
Positive cells (100%)
1.5
1.0
0.5
0.0
*
***
Cd80
Cd86
Cd206
MHC-II

Figure 4

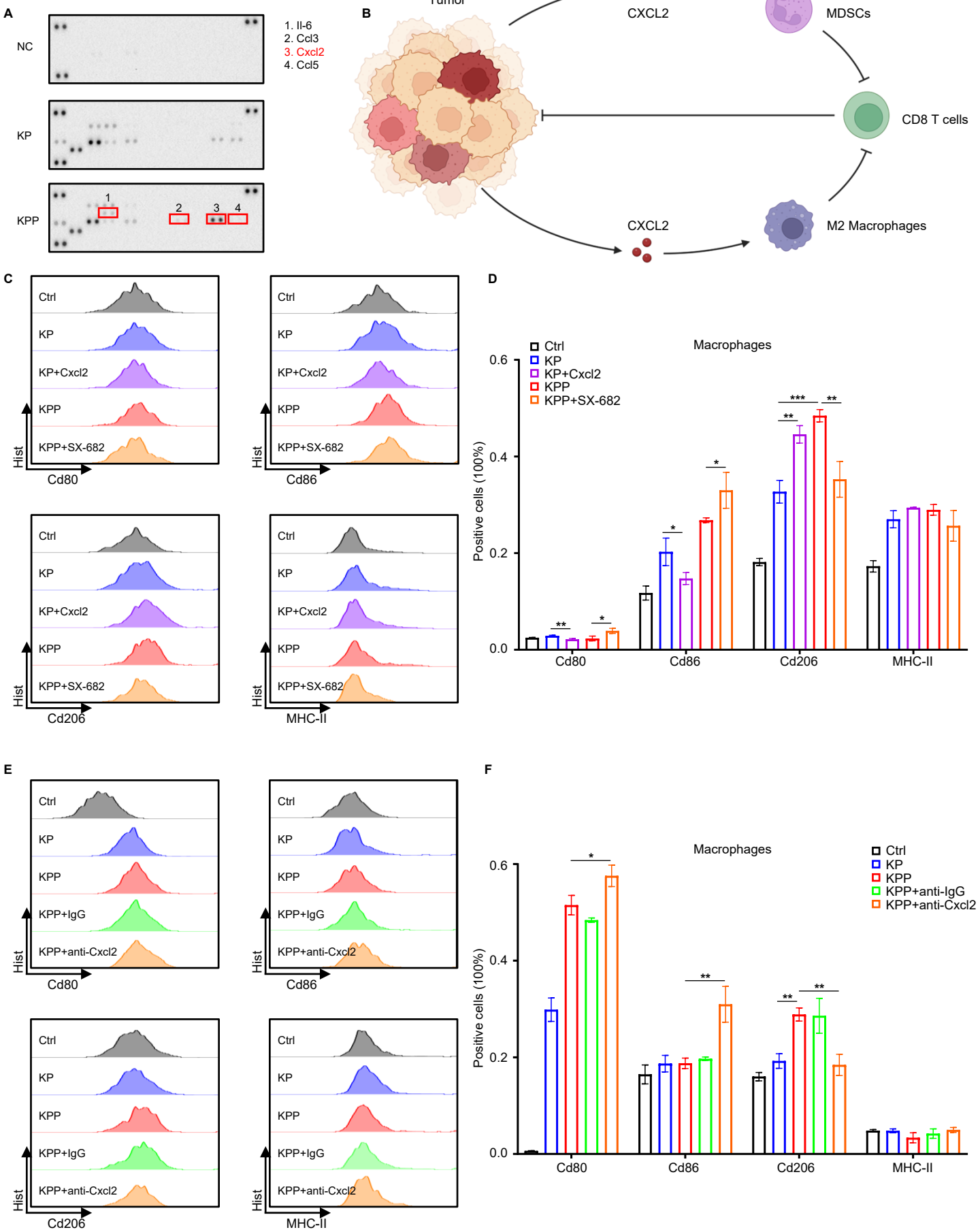
A
NC
KP
KPP
1
2
3
4
1. Il-6
2. Ccl3
3. Cxcl2
4. Ccl5
B
Tumor
CXCL2
MDSCs
CD8 T cells
CXCL2
M2 Macrophages
C
Ctrl
KP
KP+Cxcl2
KPP
KPP+SX-682
Hist
Cd80
Cd86
Cd206
MHC-II
D
Macrophages
Ctrl
KP
KP+Cxcl2
KPP
KPP+SX-682
Positive cells (100%)
0.6
0.4
0.2
0.0
Cd80
Cd86
Cd206
MHC-II
E
KPP+IgG
KPP+anti-Cxcl2
F
Macrophages
Ctrl
KP
KPP
KPP+anti-IgG
KPP+anti-Cxcl2
Positive cells (100%)
0.6
0.4
0.2
0.0
Cd80
Cd86
Cd206
MHC-II

Figure 5

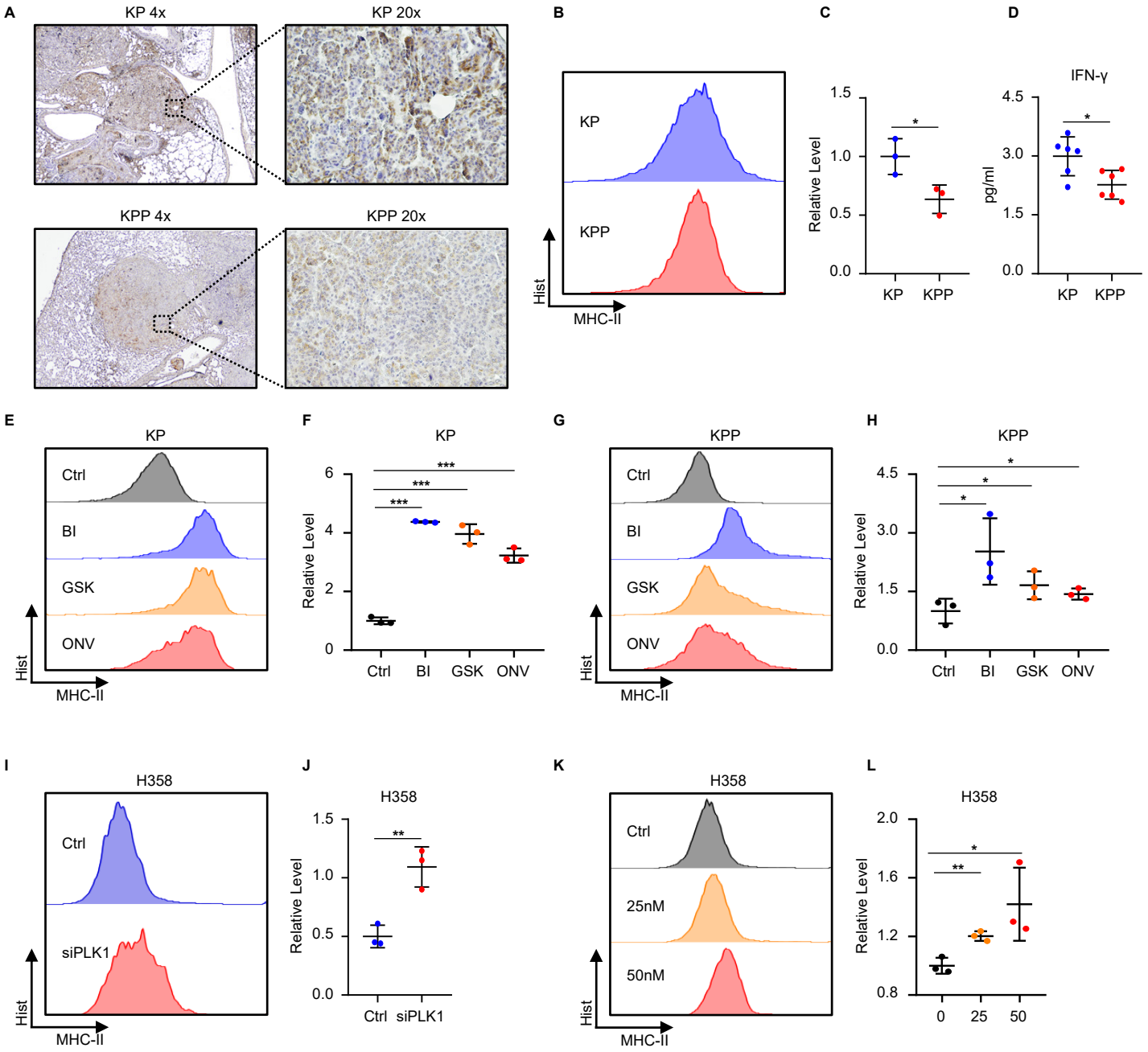
A
KP 4x
KP 20x
KPP 4x
KPP 20x
B
KP
KPP
Hist
MHC-II
C
Relative Level
1.5
1.0
0.5
0.0
*
KP
KPP
D
IFN-γ
pg/ml
4.5
3.0
1.5
0.0
*
KP
KPP
E
KP
Ctrl
BI
GSK
ONV
Hist
MHC-II
F
KP
Relative Level
6
4
2
0
***
***
***
Ctrl
BI
GSK
ONV
G
KPP
Ctrl
BI
GSK
ONV
Hist
MHC-II
H
KPP
Relative Level
4.5
3.0
1.5
0.0
*
*
*
Ctrl
BI
GSK
ONV
I
H358
Ctrl
siPLK1
Hist
MHC-II
J
H358
Relative Level
1.5
1.0
0.5
0.0
**
Ctrl
siPLK1
K
H358
Ctrl
25nM
50nM
Hist
MHC-II
L
H358
Relative Level
2.0
1.6
1.2
0.8
*
**
0
25
50

Figure 6

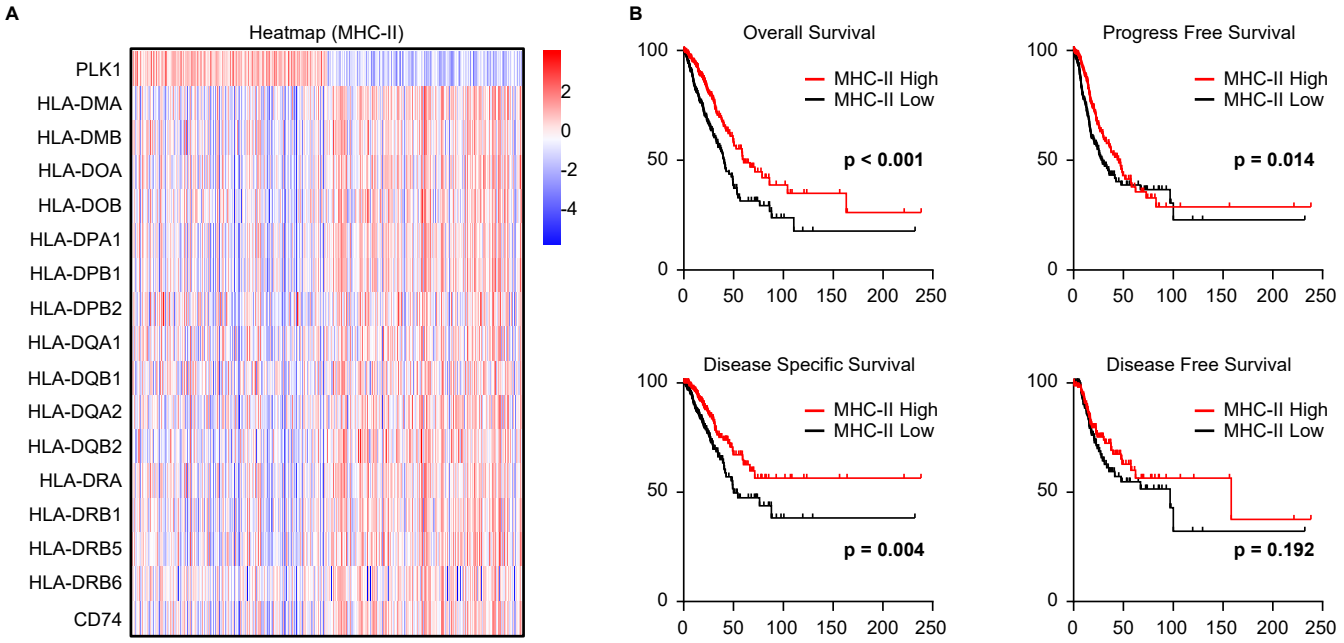
A
Heatmap (MHC-II)
PLK1
HLA-DMA
HLA-DMB
HLA-DOA
HLA-DOB
HLA-DPA1
HLA-DPB1
HLA-DPB2
HLA-DQA1
HLA-DQB1
HLA-DQA2
HLA-DQB2
HLA-DRA
HLA-DRB1
HLA-DRB5
HLA-DRB6
CD74
2
0
-2
-4
B
Overall Survival
MHC-II High
MHC-II Low
p < 0.001
Progress Free Survival
MHC-II High
MHC-II Low
p = 0.014
Disease Specific Survival
MHC-II High
MHC-II Low
p = 0.004
Disease Free Survival
MHC-II High
MHC-II Low
p = 0.192
100
50
0
0
50
100
150
200
250

Figure 7

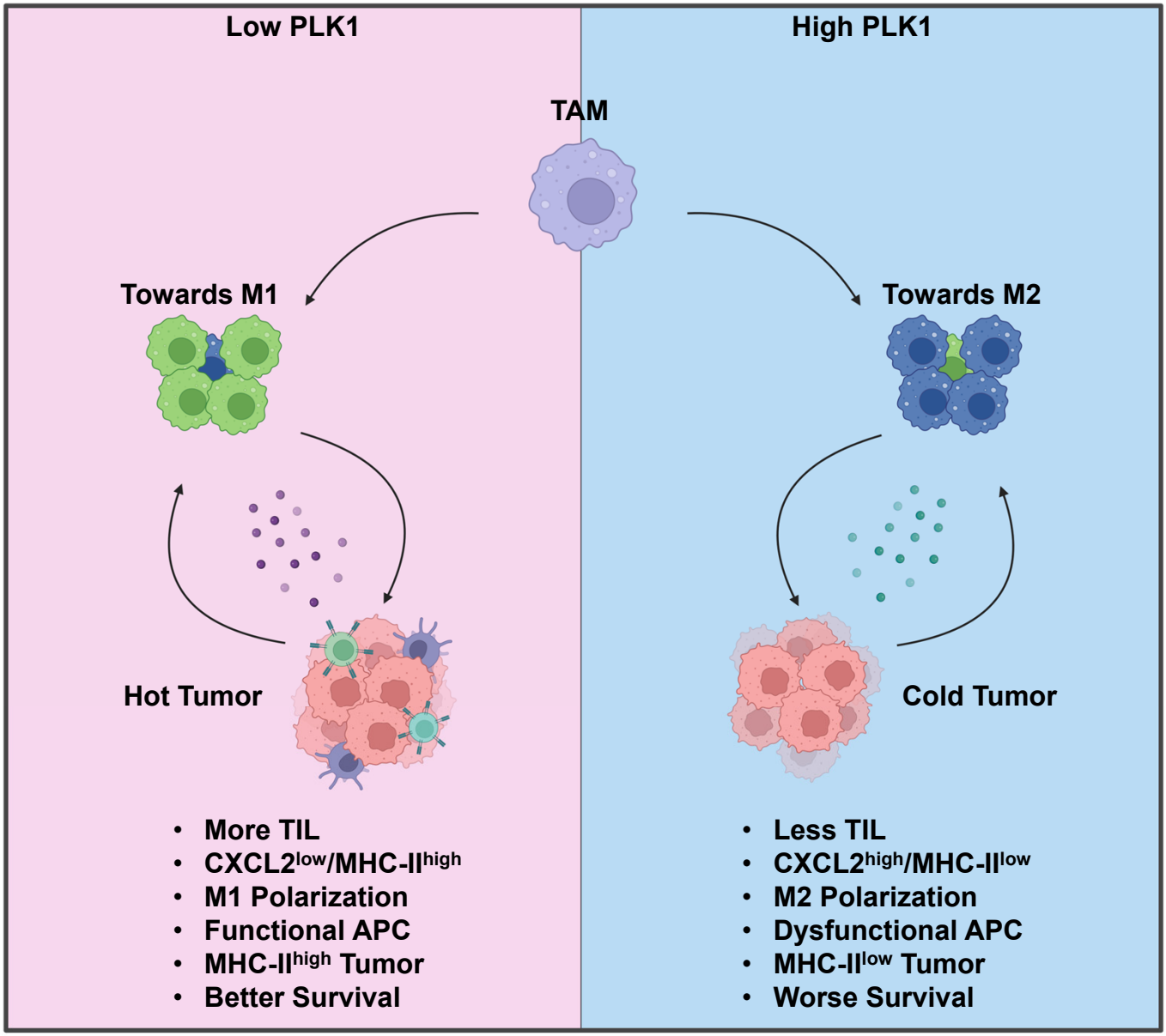
Low PLK1
High PLK1
TAM
Towards M1
Towards M2
Hot Tumor
Cold Tumor
• More TIL
• CXCL2low/MHC-IIhigh
• M1 Polarization
• Functional APC
• MHC-IIhigh Tumor
• Better Survival
• Less TIL
• CXCL2high/MHC-IIlow
• M2 Polarization
• Dysfunctional APC
• MHC-IIlow Tumor
• Worse Survival

Figure S1

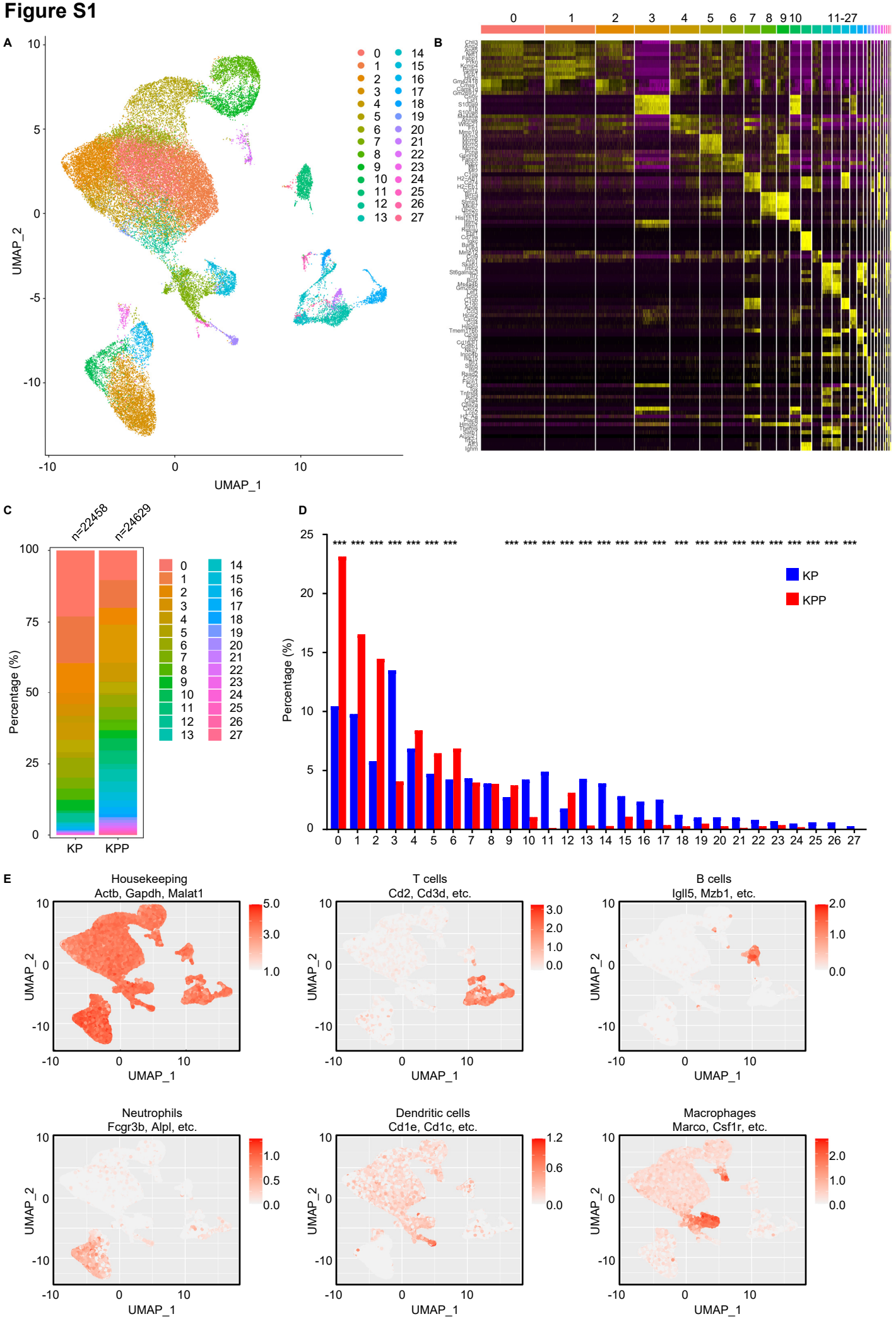
A
UMAP_2
UMAP_1
0 1 2 3 4 5 6 7 8 9 10 11 12 13 14 15 16 17 18 19 20 21 22 23 24 25 26 27
B
0 1 2 3 4 5 6 7 8 9 10 11-27
C
n=22458
n=24629
Percentage (%)
KP
KPP
D
Percentage (%)
KP
KPP
E
Housekeeping
Actb, Gapdh, Malat1
T cells
Cd2, Cd3d, etc.
B cells
Igll5, Mzb1, etc.
Neutrophils
Fcgr3b, Alpl, etc.
Dendritic cells
Cd1e, Cd1c, etc.
Macrophages
Marco, Csf1r, etc.

Figure S2

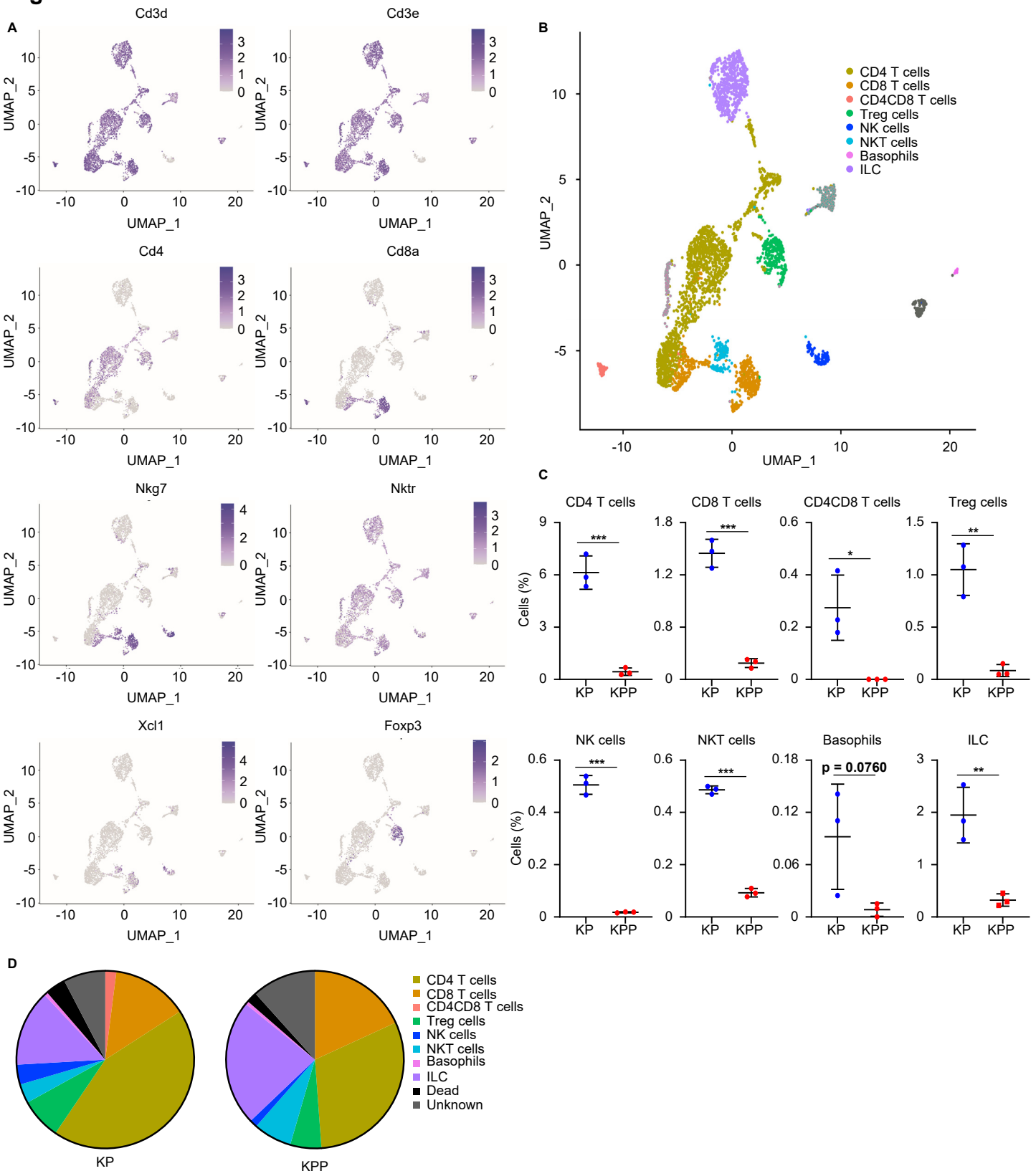
A
Cd3d
Cd3e
Cd4
Cd8a
Nkg7
Nktr
Xcl1
Foxp3
UMAP_1
UMAP_2
B
CD4 T cells
CD8 T cells
CD4CD8 T cells
Treg cells
NK cells
NKT cells
Basophils
ILC
C
Cells (%)
KP
KPP
p = 0.0760
D
Dead
Unknown

Figure S3

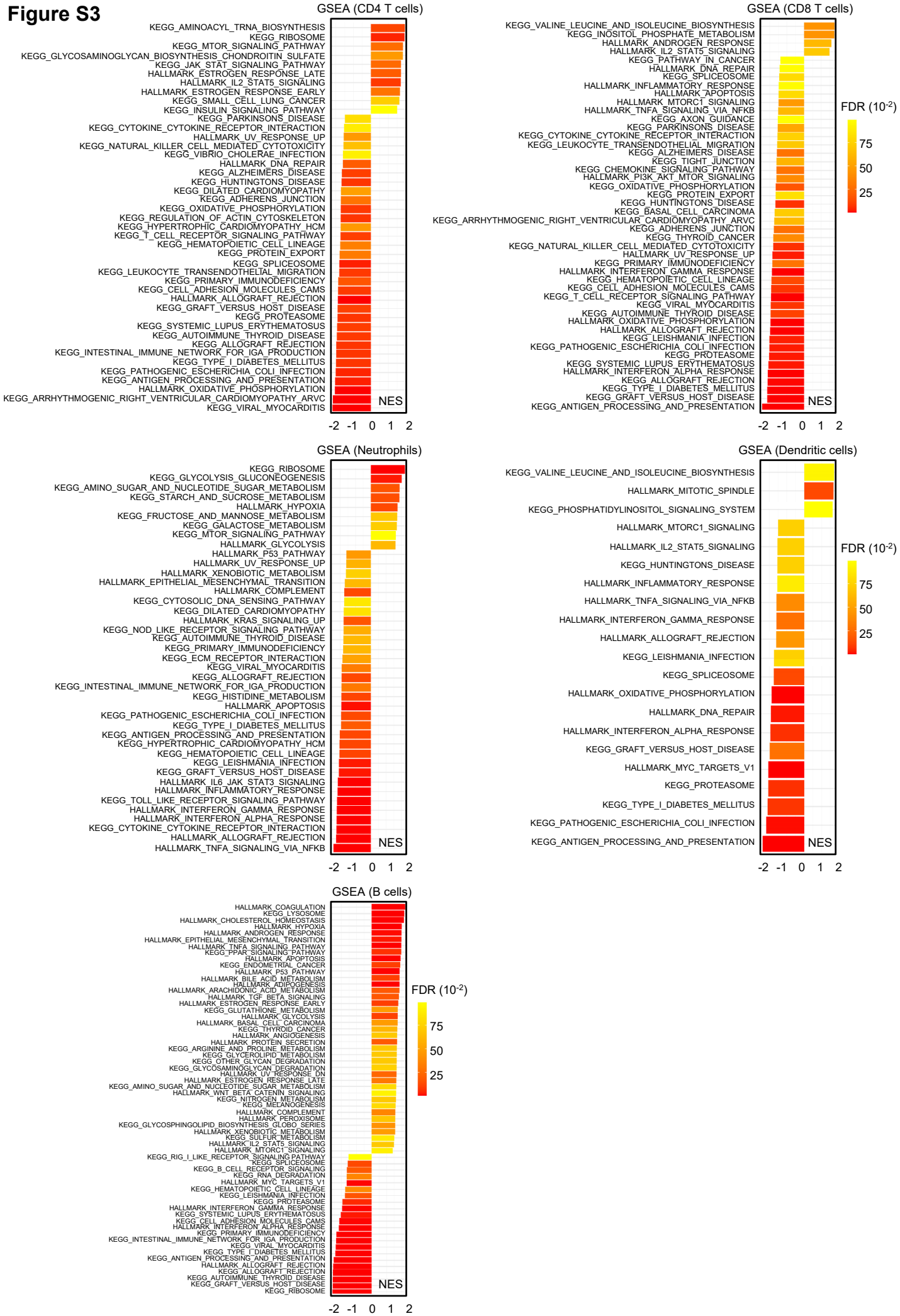
GSEA (CD4 T cells)
KEGG_AMINOACYL_TRNA_BIOSYNTHESIS
KEGG_RIBOSOME
KEGG_MTOR_SIGNALING_PATHWAY
KEGG_GLYCOSAMINOGLYCAN_BIOSYNTHESIS_CHONDROITIN_SULFATE
KEGG_JAK_STAT_SIGNALING_PATHWAY
HALLMARK_ESTROGEN_RESPONSE_LATE
HALLMARK_IL2_STAT5_SIGNALING
HALLMARK_ESTROGEN_RESPONSE_EARLY
KEGG_SMALL_CELL_LUNG_CANCER
KEGG_INSULIN_SIGNALING_PATHWAY
KEGG_PARKINSONS_DISEASE
KEGG_CYTOKINE_CYTOKINE_RECEPTOR_INTERACTION
HALLMARK_UV_RESPONSE_UP
KEGG_NATURAL_KILLER_CELL_MEDIATED_CYTOTOXICITY
KEGG_VIBRIO_CHOLERAE_INFECTION
HALLMARK_DNA_REPAIR
KEGG_ALZHEIMERS_DISEASE
KEGG_HUNTINGTONS_DISEASE
KEGG_DILATED_CARDIOMYOPATHY
KEGG_ADHERENS_JUNCTION
KEGG_OXIDATIVE_PHOSPHORYLATION
KEGG_REGULATION_OF_ACTIN_CYTOSKELETON
KEGG_HYPERTROPHIC_CARDIOMYOPATHY_HCM
KEGG_T_CELL_RECEPTOR_SIGNALING_PATHWAY
KEGG_HEMATOPOIETIC_CELL_LINEAGE
KEGG_PROTEIN_EXPORT
KEGG_SPLICEOSOME
KEGG_LEUKOCYTE_TRANSENDOTHELIAL_MIGRATION
KEGG_PRIMARY_IMMUNODEFICIENCY
KEGG_CELL_ADHESION_MOLECULES_CAMS
HALLMARK_ALLOGRAFT_REJECTION
KEGG_GRAFT_VERSUS_HOST_DISEASE
KEGG_PROTEASOME
KEGG_SYSTEMIC_LUPUS_ERYTHEMATOSUS
KEGG_AUTOIMMUNE_THYROID_DISEASE
KEGG_ALLOGRAFT_REJECTION
KEGG_INTESTINAL_IMMUNE_NETWORK_FOR_IGA_PRODUCTION
KEGG_TYPE_I_DIABETES_MELLITUS
KEGG_PATHOGENIC_ESCHERICHIA_COLI_INFECTION
KEGG_ANTIGEN_PROCESSING_AND_PRESENTATION
HALLMARK_OXIDATIVE_PHOSPHORYLATION
KEGG_ARRHYTHMOGENIC_RIGHT_VENTRICULAR_CARDIOMYOPATHY_ARVC
KEGG_VIRAL_MYOCARDITIS
NES
-2 -1 0 1 2
GSEA (CD8 T cells)
KEGG_VALINE_LEUCINE_AND_ISOLEUCINE_BIOSYNTHESIS
KEGG_INOSITOL_PHOSPHATE_METABOLISM
HALLMARK_ANDROGEN_RESPONSE
HALLMARK_IL2_STAT5_SIGNALING
KEGG_PATHWAY_IN_CANCER
HALLMARK_DNA_REPAIR
KEGG_SPLICEOSOME
HALLMARK_INFLAMMATORY_RESPONSE
HALLMARK_APOPTOSIS
HALLMARK_MTORC1_SIGNALING
HALLMARK_TNFA_SIGNALING_VIA_NFKB
KEGG_AXON_GUIDANCE
KEGG_PARKINSONS_DISEASE
KEGG_CYTOKINE_CYTOKINE_RECEPTOR_INTERACTION
KEGG_LEUKOCYTE_TRANSENDOTHELIAL_MIGRATION
KEGG_ALZHEIMERS_DISEASE
KEGG_TIGHT_JUNCTION
KEGG_CHEMOKINE_SIGNALING_PATHWAY
HALLMARK_PI3K_AKT_MTOR_SIGNALING
KEGG_OXIDATIVE_PHOSPHORYLATION
KEGG_PROTEIN_EXPORT
KEGG_HUNTINGTONS_DISEASE
KEGG_BASAL_CELL_CARCINOMA
KEGG_ARRHYTHMOGENIC_RIGHT_VENTRICULAR_CARDIOMYOPATHY_ARVC
KEGG_ADHERENS_JUNCTION
KEGG_THYROID_CANCER
KEGG_NATURAL_KILLER_CELL_MEDIATED_CYTOTOXICITY
HALLMARK_UV_RESPONSE_UP
KEGG_PRIMARY_IMMUNODEFICIENCY
HALLMARK_INTERFERON_GAMMA_RESPONSE
KEGG_HEMATOPOIETIC_CELL_LINEAGE
KEGG_CELL_ADHESION_MOLECULES_CAMS
KEGG_T_CELL_RECEPTOR_SIGNALING_PATHWAY
KEGG_VIRAL_MYOCARDITIS
KEGG_AUTOIMMUNE_THYROID_DISEASE
HALLMARK_OXIDATIVE_PHOSPHORYLATION
HALLMARK_ALLOGRAFT_REJECTION
KEGG_LEISHMANIA_INFECTION
KEGG_PATHOGENIC_ESCHERICHIA_COLI_INFECTION
KEGG_PROTEASOME
KEGG_SYSTEMIC_LUPUS_ERYTHEMATOSUS
HALLMARK_INTERFERON_ALPHA_RESPONSE
KEGG_ALLOGRAFT_REJECTION
KEGG_TYPE_I_DIABETES_MELLITUS
KEGG_GRAFT_VERSUS_HOST_DISEASE
KEGG_ANTIGEN_PROCESSING_AND_PRESENTATION
NES
-2 -1 0 1 2
FDR (10-2)
75
50
25
GSEA (Neutrophils)
KEGG_RIBOSOME
KEGG_GLYCOLYSIS_GLUCONEOGENESIS
KEGG_AMINO_SUGAR_AND_NUCLEOTIDE_SUGAR_METABOLISM
KEGG_STARCH_AND_SUCROSE_METABOLISM
HALLMARK_HYPOXIA
KEGG_FRUCTOSE_AND_MANNOSE_METABOLISM
KEGG_GALACTOSE_METABOLISM
KEGG_MTOR_SIGNALING_PATHWAY
HALLMARK_GLYCOLYSIS
HALLMARK_P53_PATHWAY
HALLMARK_UV_RESPONSE_UP
HALLMARK_XENOBIOTIC_METABOLISM
HALLMARK_EPITHELIAL_MESENCHYMAL_TRANSITION
HALLMARK_COMPLEMENT
KEGG_CYTOSOLIC_DNA_SENSING_PATHWAY
KEGG_DILATED_CARDIOMYOPATHY
HALLMARK_KRAS_SIGNALING_UP
KEGG_NOD_LIKE_RECEPTOR_SIGNALING_PATHWAY
KEGG_AUTOIMMUNE_THYROID_DISEASE
KEGG_PRIMARY_IMMUNODEFICIENCY
KEGG_ECM_RECEPTOR_INTERACTION
KEGG_VIRAL_MYOCARDITIS
KEGG_ALLOGRAFT_REJECTION
KEGG_INTESTINAL_IMMUNE_NETWORK_FOR_IGA_PRODUCTION
KEGG_HISTIDINE_METABOLISM
HALLMARK_APOPTOSIS
KEGG_PATHOGENIC_ESCHERICHIA_COLI_INFECTION
KEGG_TYPE_I_DIABETES_MELLITUS
KEGG_ANTIGEN_PROCESSING_AND_PRESENTATION
KEGG_HYPERTROPHIC_CARDIOMYOPATHY_HCM
KEGG_HEMATOPOIETIC_CELL_LINEAGE
KEGG_LEISHMANIA_INFECTION
KEGG_GRAFT_VERSUS_HOST_DISEASE
HALLMARK_IL6_JAK_STAT3_SIGNALING
HALLMARK_INFLAMMATORY_RESPONSE
KEGG_TOLL_LIKE_RECEPTOR_SIGNALING_PATHWAY
HALLMARK_INTERFERON_GAMMA_RESPONSE
HALLMARK_INTERFERON_ALPHA_RESPONSE
KEGG_CYTOKINE_CYTOKINE_RECEPTOR_INTERACTION
HALLMARK_ALLOGRAFT_REJECTION
HALLMARK_TNFA_SIGNALING_VIA_NFKB
NES
-2 -1 0 1 2
GSEA (Dendritic cells)
KEGG_VALINE_LEUCINE_AND_ISOLEUCINE_BIOSYNTHESIS
HALLMARK_MITOTIC_SPINDLE
KEGG_PHOSPHATIDYLINOSITOL_SIGNALING_SYSTEM
HALLMARK_MTORC1_SIGNALING
HALLMARK_IL2_STAT5_SIGNALING
KEGG_HUNTINGTONS_DISEASE
HALLMARK_INFLAMMATORY_RESPONSE
HALLMARK_TNFA_SIGNALING_VIA_NFKB
HALLMARK_INTERFERON_GAMMA_RESPONSE
HALLMARK_ALLOGRAFT_REJECTION
KEGG_LEISHMANIA_INFECTION
KEGG_SPLICEOSOME
HALLMARK_OXIDATIVE_PHOSPHORYLATION
HALLMARK_DNA_REPAIR
HALLMARK_INTERFERON_ALPHA_RESPONSE
KEGG_GRAFT_VERSUS_HOST_DISEASE
HALLMARK_MYC_TARGETS_V1
KEGG_PROTEASOME
KEGG_TYPE_I_DIABETES_MELLITUS
KEGG_PATHOGENIC_ESCHERICHIA_COLI_INFECTION
KEGG_ANTIGEN_PROCESSING_AND_PRESENTATION
NES
-2 -1 0 1 2
FDR (10-2)
75
50
25
GSEA (B cells)
HALLMARK_COAGULATION
KEGG_LYSOSOME
HALLMARK_CHOLESTEROL_HOMEOSTASIS
HALLMARK_HYPOXIA
HALLMARK_ANDROGEN_RESPONSE
HALLMARK_EPITHELIAL_MESENCHYMAL_TRANSITION
HALLMARK_TNFA_SIGNALING_PATHWAY
KEGG_PPAR_SIGNALING_PATHWAY
HALLMARK_APOPTOSIS
KEGG_ENDOMETRIAL_CANCER
HALLMARK_P53_PATHWAY
HALLMARK_BILE_ACID_METABOLISM
HALLMARK_ADIPOGENESIS
HALLMARK_ARACHIDONIC_ACID_METABOLISM
HALLMARK_TGF_BETA_SIGNALING
HALLMARK_ESTROGEN_RESPONSE_EARLY
KEGG_GLUTATHIONE_METABOLISM
HALLMARK_GLYCOLYSIS
HALLMARK_BASAL_CELL_CARCINOMA
KEGG_THYROID_CANCER
HALLMARK_ANGIOGENESIS
HALLMARK_PROTEIN_SECRETION
KEGG_ARGININE_AND_PROLINE_METABOLISM
KEGG_GLYCEROLIPID_METABOLISM
KEGG_OTHER_GLYCAN_DEGRADATION
KEGG_GLYCOSAMINOGLYCAN_DEGRADATION
HALLMARK_UV_RESPONSE_DN
HALLMARK_ESTROGEN_RESPONSE_LATE
KEGG_AMINO_SUGAR_AND_NUCLEOTIDE_SUGAR_METABOLISM
HALLMARK_WNT_BETA_CATENIN_SIGNALING
KEGG_NITROGEN_METABOLISM
KEGG_MELANOGENESIS
HALLMARK_COMPLEMENT
HALLMARK_PEROXISOME
KEGG_GLYCOSPHINGOLIPID_BIOSYNTHESIS_GLOBO_SERIES
HALLMARK_XENOBIOTIC_METABOLISM
KEGG_SULFUR_METABOLISM
HALLMARK_IL2_STAT5_SIGNALING
HALLMARK_MTORC1_SIGNALING
KEGG_RIG_I_LIKE_RECEPTOR_SIGNALING_PATHWAY
KEGG_SPLICEOSOME
KEGG_B_CELL_RECEPTOR_SIGNALING
KEGG_RNA_DEGRADATION
HALLMARK_MYC_TARGETS_V1
KEGG_HEMATOPOIETIC_CELL_LINEAGE
KEGG_LEISHMANIA_INFECTION
KEGG_PROTEASOME
HALLMARK_INTERFERON_GAMMA_RESPONSE
KEGG_SYSTEMIC_LUPUS_ERYTHEMATOSUS
KEGG_CELL_ADHESION_MOLECULES_CAMS
HALLMARK_INTERFERON_ALPHA_RESPONSE
KEGG_PRIMARY_IMMUNODEFICIENCY
KEGG_INTESTINAL_IMMUNE_NETWORK_FOR_IGA_PRODUCTION
KEGG_VIRAL_MYOCARDITIS
KEGG_TYPE_I_DIABETES_MELLITUS
KEGG_ANTIGEN_PROCESSING_AND_PRESENTATION
HALLMARK_ALLOGRAFT_REJECTION
KEGG_ALLOGRAFT_REJECTION
KEGG_AUTOIMMUNE_THYROID_DISEASE
KEGG_GRAFT_VERSUS_HOST_DISEASE
KEGG_RIBOSOME
NES
-2 -1 0 1 2
FDR (10-2)
75
50
25

Figure S4

A

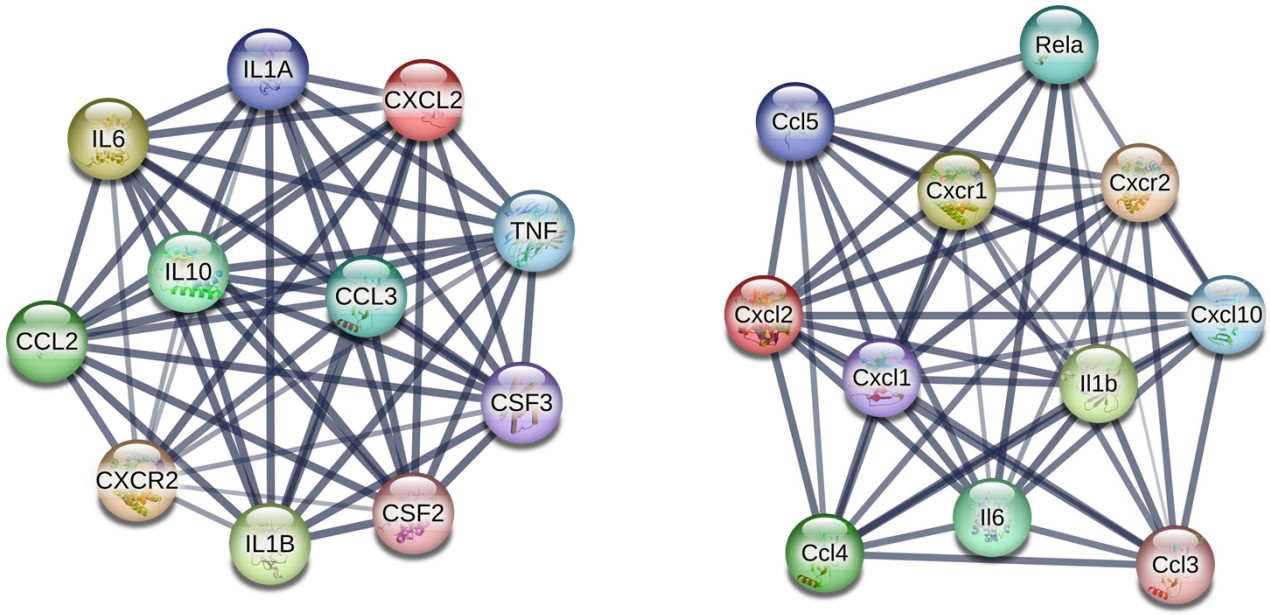

B

GSEA of RNA-seq: GSE206644 (KPP vs KP)		
	HALLMARK_ IL6_JAK_STAT3_SIGNALING	**HALLMARK_ TNFA_SIGNALING_VIA_NFKB**
NES	1.56	1.52
FDR	**0.023**	**0.028**

Figure S5

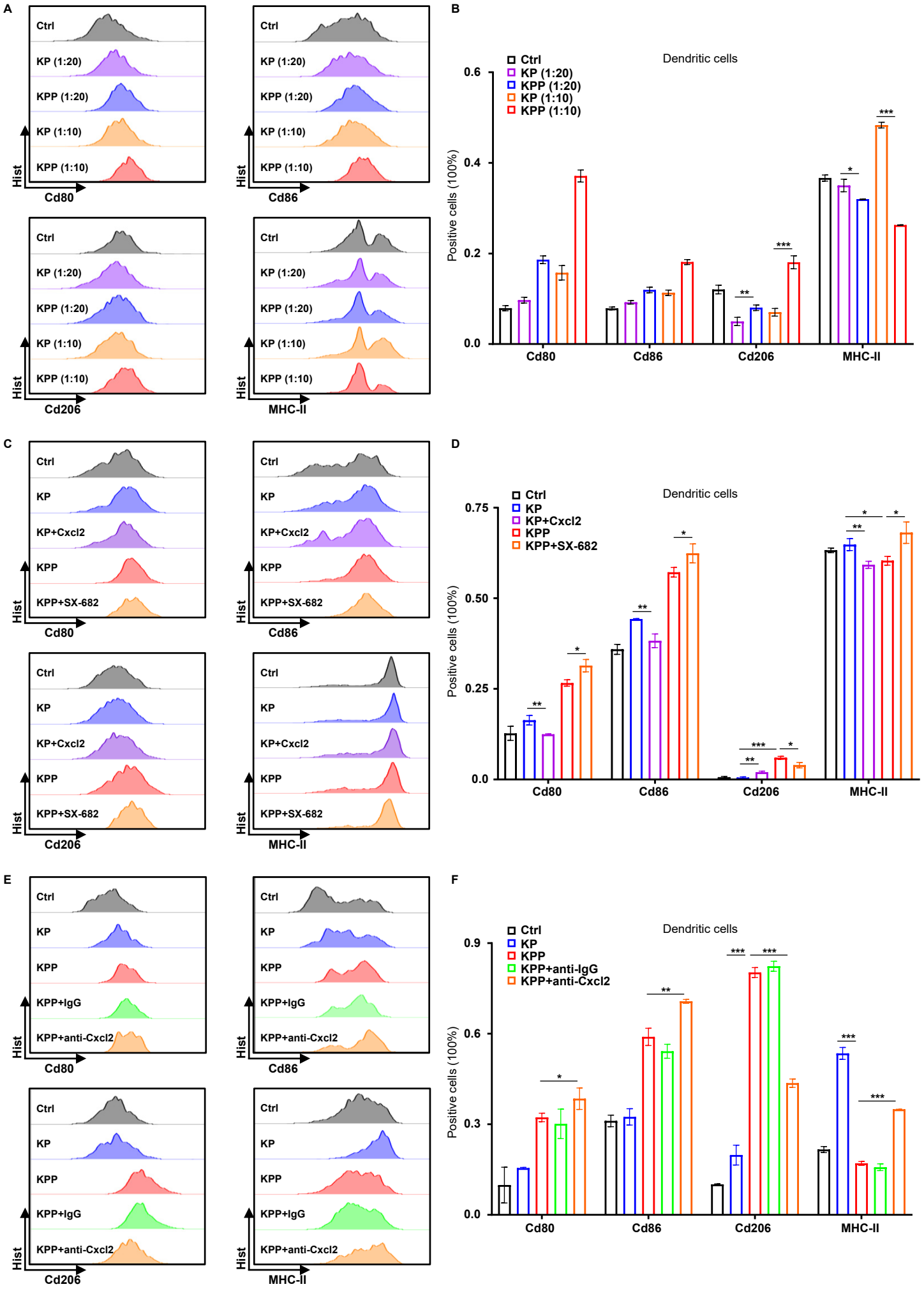
A
Ctrl
KP (1:20)
KPP (1:20)
KP (1:10)
KPP (1:10)
Hist
Cd80
Cd86
Cd206
MHC-II
B
Dendritic cells
Positive cells (100%)
0.6
0.4
0.2
0.0
Cd80
Cd86
Cd206
MHC-II
C
Ctrl
KP
KP+Cxcl2
KPP
KPP+SX-682
D
Dendritic cells
Positive cells (100%)
0.75
0.50
0.25
0.0
E
Ctrl
KP
KPP
KPP+IgG
KPP+anti-Cxcl2
F
Dendritic cells
Positive cells (100%)
0.9
0.6
0.3
0.0

Figure S6

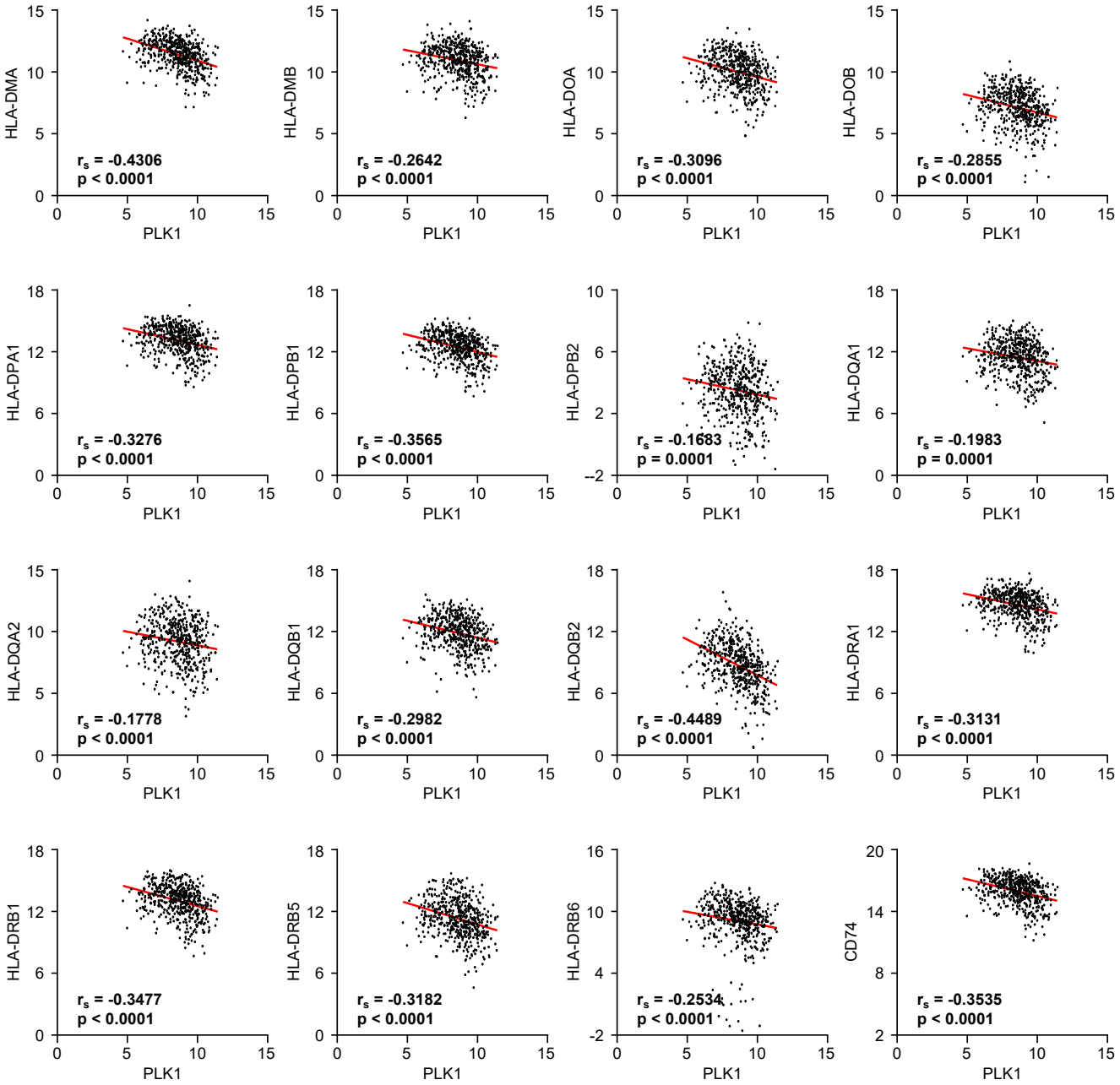
HLA-DMA
r_s = -0.4306
p < 0.0001
HLA-DMB
r_s = -0.2642
p < 0.0001
HLA-DOA
r_s = -0.3096
p < 0.0001
HLA-DOB
r_s = -0.2855
p < 0.0001
HLA-DPA1
r_s = -0.3276
p < 0.0001
HLA-DPB1
r_s = -0.3565
p < 0.0001
HLA-DPB2
r_s = -0.1683
p = 0.0001
HLA-DQA1
r_s = -0.1983
p = 0.0001
HLA-DQA2
r_s = -0.1778
p < 0.0001
HLA-DQB1
r_s = -0.2982
p < 0.0001
HLA-DQB2
r_s = -0.4489
p < 0.0001
HLA-DRA1
r_s = -0.3131
p < 0.0001
HLA-DRB1
r_s = -0.3477
p < 0.0001
HLA-DRB5
r_s = -0.3182
p < 0.0001
HLA-DRB6
r_s = -0.2534
p < 0.0001
CD74
r_s = -0.3535
p < 0.0001
PLK1